

Mono Lake or Laschamp geomagnetic event recorded from lava flows in Amsterdam Island (southeastern Indian Ocean).

Claire Carvallo^{1*}, Pierre Camps^{1†}, Gilles Ruffet², Bernard Henry³ & T. Poidras¹

¹*Laboratoire de Tectonophysique, CNRS and ISTEEM, Université Montpellier 2, Montpellier, France*

²*CNRS and Géosciences Rennes, Université de Rennes 1, Rennes, France*

³*Laboratoire Géomagnétisme et Paléomagnétisme, CNRS and IPGP, Paris, France.*

under press in *Geophysical Journal International*

April 17th, 2003

SUMMARY

We report a survey carried out on basalt flows from Amsterdam Island (Southeastern Indian Ocean) in order to check the presence of intermediate directions interpreted to belong to a geomagnetic field excursion within the Brunhes epoch (Watkins & Nougier, 1973), completing this paleomagnetic record with paleointensity determinations and radiometric dating. Because the paleomagnetic sampling was done in few hours during the re-supply of the French scientific base Martin du Vivier by the Marion Dufresne vessel, we could collect only 29 samples from 4 lava flows. The directional results corroborate the findings by Watkins & Nougier (1973) : normal polarity is found for two units and an intermediate direction, with associated Virtual Geomagnetic Poles (VGPs) close to the equator, for the other two units. A notable result is that these volcanic rocks are well suited for absolute paleointensity determinations. Fifty percent of the samples yields reliable intensity values with high quality factors. An original element of this study is that we made use of the thermomagnetic criterion PTRM-tail test of Shcherbakova et

al. (2000) to help in the interpretation of the paleointensity measurements. Doing thus, only the high temperature intervals, beyond 400°C, were retained to obtain the most reliable estimate of the strength of the ancient magnetic field. However, not applying the PTRM-tail test does not change the flow-mean values significantly because the samples we selected by conventional criteria for estimating the paleointensity carry only a small proportion of their remanence below 400°C. The normal units yield Virtual Dipole Moments (VDM) of 6.2 and 7.7 (10^{22}Am^2) and the excursion units yield values of 3.7 and 3.4 (10^{22}Am^2). These results are quite consistent with the other Thellier determinations from Brunhes excursion records, all characterized by a decrease of the VDM as VGP latitude decreases. $^{40}\text{Ar}/^{39}\text{Ar}$ isotopic age determinations provide an estimate of 26 ± 15 Kyr and 18 ± 9 Kyr for the transitional lava flows, which could correspond to the Mono Lake excursion. However, the large error bars associated with these ages do not exclude the hypothesis that this event is the Laschamp.

Key words: Geomagnetic excursion, Mono Lake, Laschamp, Paleointensity, $^{40}\text{Ar}/^{39}\text{Ar}$ dating, Amsterdam Island.

1 INTRODUCTION

Just over twenty years ago Hoffman (1981) concluded from the characteristics of the Earth's magnetic field observed during geomagnetic excursions that at least some excursions are aborted reversals. This implies that paleomagnetic field variations derived from such records can be interpreted as transitional fields. Recently, Gubbins (1999) proposed a physical explanation to this hypothesis. According to Gubbins excursions may occur when two reversals of opposite sense follow one another in the liquid outer core, which has timescales of about 500 yr, within such a short time interval that the field does not have enough time to reverse its polarity in the solid inner core, which occurs by diffusion with typical timescales of 3 Kyr. In other words, he considers that the longer dynamical timescales of the solid inner core delay

*Now at Geophysics, Department of Physics, University of Toronto, Canada

†Corresponding author. Tel: +33 467 14 39 38; Email: camps@dstu.univ-montp2.fr

full reversals which are not complete until the magnetic field reverses its polarity throughout the whole Earth's core. This physical distinction between successful and unsuccessful reversals agrees with both the duration of excursions, estimated at a few thousands years, and with their number of about ten observed within the Brunhes period (from 780 Kyr to present time) (Langereis et al., 1997). To validate such models one must know the exact duration of excursions and the frequency of their occurrences between two consecutive full reversals. However even for the Brunhes period, we are not yet able to precisely describe the excursion succession and their individual characteristics. Some excursions are not clearly established, the global occurrence of some others is questioned (Langereis et al., 1997). For example, the Mono Lake excursion (≈ 28 ka) is observed only in sediments from the western North America (Liddicoat & Coe, 1979; Levi & Karlin, 1989; Liddicoat, 1992; Liddicoat, 1996) and from Arctic Sea (Nowaczyk & Antonow, 1997) and thus may only reflect a strong regional secular variation feature. To date only 6 excursions within the Brunhes period seem well established, accurately dated and appear to occur globally. This is the case for Laschamp (40-45 Ka), Blake (110-120 Ka), Jamaica/Pringle Falls (218 ± 10 ka), Calabrian Ridge 1 (315-325 ka) and 2 (515-525 ka) and Emperor/Big Lost (560-570 ka) (see e.g. Langereis et al. (1997) and reference therein for a review). Nevertheless it is not yet completely ascertained whether global excursions are synchronous all over the globe or start at some locations before spreading over the entire core surface. The answer to this question is of importance for both geodynamo models and correlations of high resolution sedimentary sequences. Furthermore, the available data set is somewhat incomplete: most of the excursions have been mainly described from recordings in sediments which are less reliable than volcanic rocks in term of paleodirection, particularly when the field intensity is low, which is a common characteristic of the Brunhes excursions (Guyodo & Valet, 1999). It is however not surprising that the volcanic recordings are rare, since due to the sporadic character of the volcanic extrusion rate and the short duration assumed for excursions, the probability that a lava flow occurs during an excursion is very small. As a consequence, few studies have been carried out on absolute paleointensities during Brunhes excursions (Roperch et al., 1988;

Chauvin et al., 1989; Levi et al., 1990; Quidelleur et al., 1999; Schnepf & Hradetzky, 1994; Zhu et al., 2000).

In this context, we decided to reexamine a geomagnetic excursion supposed to belong to the Brunhes period and previously described by Watkins & Nougier (1973) in lava flows from Amsterdam Island (southeastern Indian Ocean). This event has never been radiometrically dated. Our objectives were first to complete the paleomagnetic record with paleointensity determinations and to identify this geomagnetic event by radiometric dating. We also wanted to check the presence of excursion directions. In this paper we report directional results and high quality paleointensity determinations for four lava flows from Amsterdam Island. These results combined with $^{40}\text{Ar}/^{39}\text{Ar}$ isotopic ages provide more concrete evidence for the occurrence of a geomagnetic excursion recorded in Amsterdam lava during the late Pleistocene which may corresponds either to Mono Lake or Laschamp.

2 GEOLOGICAL SETTING AND PALEOMAGNETIC SAMPLING

Amsterdam Island stands where a mantle plume is interacting with a migrating mid-ocean ridge (Small, 1995). Amsterdam/Saint-Paul plateau was built within the past 4 Ma since the South East Indian Ridge (SEIR) passed over the Amstardam/Saint-Paul hotspot (Royer & Schlich, 1988). Currently, Amsterdam Island (37.5°S , 77.3°E) is located 50 km southwest of the SEIR, which is migrating to the northeast away from the plume. Lying on the nearly stationary Antarctic plate, it has been suggested that the Amsterdam/Saint-Paul plateau is still forming (Graham et al., 1999) and that volcanic risk still exists at Amsterdam and Saint Paul Islands (Johnson et al., 2000). Thus located in the immediate vicinity of a mid-ocean ridge, lava from Amsterdam has mainly tholeiitic geochemical composition, ranging from olivine tholeiite to plagioclase basalt. From a structural point of view, this volcanic island corresponds to a double strato-volcano (Gunn et al., 1971). The first cycle of activity is represented by a volcano centered on the southern part of the island, where Mount du Fernand and Le Pinion correspond to remnants of a volcanic caldera (Fig. 1). The west flank of this early volcano collapsed along two main faults oriented NW-SE and NE-SW, respectively,

creating about 800 m vertical offset and an unreachable escarpment that exposes a multitude of thin lava flows. The second cycle of activity built the Mount de la Dives volcano, which is a simple almost symmetrical volcanic cone rising to 881 m above sea level. This episode represents a displacement of the eruptive center of 2 km toward the east-northeast. The caldera on top of this young cone preserves evidence of a lava lake filled by several episodes of lava effusion which overspilled as voluminous, pahoehoe lava flows. The flanks of this volcano have regular slopes, 7 to 13°, and are not dissected by erosion. Marine erosion has formed a cliff 25-50 m high at sea level around the island which makes access from the sea difficult. Although radiometric ages were not available before the present study, the nearly-pristine morphology leaves no doubt that this volcanic activity is recent. Some parasitic cinder cones exist on the lower flanks of Mount de la Dives volcano. The youngest one is supposed to be formed during the last century.

The paleomagnetic samples were taken in few hours during the resupply of the permanent scientific station by the Marion-Dufresne vessel. Because of the limited schedule, we decided to confine the sampling to the northwestern coast where Watkins & Nougier (1973) studied six lava flows in a restricted area. Four of these flows provided excursion directions. We grouped Watkins & Nougier's (1973) flows 17 and 18, because of their confusing boundary geometries, into a single unit (am1). Probably they constitute a compound lava flow corresponding to a single volcanic eruption. Their flow 19, herein called am2, is located several meters above and corresponds undoubtly to a different volcanic eruption. Unfortunately, we were not able to reach Watkins & Nougier's (1973) flows 13, 14, and 15, because of the presence in this sector of numerous fur seals which made the access dangerous. Instead, we sampled two previously-unstudied flows (am3 and am4; Fig. 1). Seven cores from each of flows am1-2-4 and eight from flow am3 were drilled using a gasoline-powered portable drill and were oriented with respect to geographic north by means of both solar sightings and magnetic compass plus a clinometer. Based on stratigraphic relationships, all four sampled volcanic units belong to the youngest flows of the Mount de la Dives volcano. On the basis

of field observations, flow am4 is certainly younger than the other three. We have, on the other hand, no way to decipher the age relations between flows am1-2 and flow am3.

3 PALEODIRECTION DETERMINATIONS

3.1 Experimental procedure

For the analysis of remanence direction, we first treated a pilot sample from each flow using a detailed experimental procedure involving up to 13 alternating fields (AF) cleaning steps in order to check the possible presence of unstable components of remanence. Because of the simple behavior of remanence upon cleaning (Fig. 2), we used only 4 or 5 AF steps for the remaining samples. Measurements of remanent magnetization were carried out with a JR-5A spinner magnetometer and the AF treatments, with a laboratory built AF demagnetizer in which the sample is stationary and subjected to peak fields up to 140 mT. The analysis of the demagnetization diagrams is straightforward for all the samples but one, sample 693 from flows am3 was contaminated by a significant parasitic magnetization of unknown origin. We determined the Characteristic Remanent Magnetization (ChRM) by means of the principal component analysis using the Maximum Angular Deviation (MAD) (Kirschvink, 1980) as a measure of the inherent scatter in directions. In order to check if the principal component is a robust estimate of the sample ChRM, we compared this direction with the fitting line constrained through the origin. When the angle between these two directions exceeds the MAD (Audunsson & Levi, 1997) we concluded that the principal component is statistically different from the ChRM, and thus that the ChRM is not perfectly isolated. This method led to the rejection of only one sample (693) from further analysis, considering that no ChRM could be successfully determined for this sample. We averaged the directions thus obtained by flow, and calculated the statistical parameters assuming a fisherian distribution (Table 1). The ChRM directions are well clustered in each flow with rather small values of the 95 % confidence cone about the mean direction (α_{95}), all $\leq 5^\circ$.

3.2 Paleodirection results

The directional results obtained for flows am1 and am2 corroborate exactly the finding by Watkins & Nougier (1973): an intermediate polarity with associated Virtual Geomagnetic Poles (VGPs) close to the equator is found. This result is not surprising insofar as the remanence of the lava from Amsterdam is not contaminated by significant spurious components. This was not the case, for example, in a recent study on the volcanic sequence from Possession Island (Camps et al., 2001), where the authors concluded that the intermediate directions initially described by Watkins et al. (1972) correspond to reversed directions which had been incompletely cleaned of their present-day field viscous overprint. Here, we believe that the previously published data for Amsterdam Island (Watkins & Nougier, 1973), which were not resampled in the present study are, equally reliable.

Because flows am1 and am2 yield two similar directions and because they are in a single sequence on a small cliff, one can ask whether the time elapsed between these two flows is long enough to consider them separately. To try to reply briefly, we performed the bootstrap test for a common mean (Tauxe, 1998). Because the 95 % bound interval for the Cartesian Y and Z coordinates calculated for these two directions do not overlap each other (Fig. 3), we concluded that these directions are statistically different and thus can be analyzed individually. Flows am3 and am4 give normal directions. They can be used to complete Watkins & Nougier's (1973) dataset in order to estimate the amplitude of secular variation from the Indian Ocean for the Brunhes period.

4 PALEOINTENSITY DETERMINATIONS

4.1 Experimental procedure

Paleointensity determinations were carried out using the classical Thellier and Thellier (1959) method. The samples are heated two times at each temperature step, in the presence of a field positive for the first heating and negative for the second heating. Partial thermore-

manent magnetization (pTRM) checks were performed every two steps in order to detect magnetic changes during heating. We used a laboratory field of $30 \mu\text{T}$ aligned along the core z axis. All heatings and coolings were done in a vacuum better than 10^{-4} mbar with the intention of reducing mineralogical changes during heatings, which are usually due to oxidation. Samples were heated in 14 steps between 150 and 580 °C, by 50°C between 150 and 500 °C, then 20°C steps between 500 and 540°C, and finally 10°C steps between 540 and 580°C. Each heating-cooling step required about 10 hours. Because paleointensity measurements require time-consuming procedures, it is important to detect unsuitable samples before carrying out the full experiments.

4.2 Sample selection and rock magnetism properties

Volcanic rocks used for absolute paleointensity determinations must satisfy the following conditions :

- (i) The natural remanent magnetization (NRM) of samples must consist of a single component close to the mean characteristic remanence direction of the flow. In addition, the viscosity index (Thellier & Thellier, 1944) must be small enough to obtain reliable data during the heating demagnetization steps at low temperatures. We found that all the samples have magnetic viscosity coefficients smaller than 4%; therefore no samples were eliminated on this basis, except sample 693 which shows a strong secondary component of magnetization.
- (ii) The magnetic properties of the samples must be thermally stable. To check it, we performed continuous low-field magnetic susceptibility measurements under vacuum (better than 10^{-2} mbar) as a function of temperature (Fig. 4) for the 28 remaining samples. The device used for this experiment is a Bartington susceptibility meter MS2 equipped with a furnace in which the heating and cooling rates remain constant at 7°/mn. Seven samples having irreversible thermomagnetic curves were rejected for the final selection of paleointensity results. Mean Curie temperatures (Prévot et al., 1983) vary between 450 and 570°C (Table 2). These values also indicate that the magnetic carriers are mainly Ti-poor titanomagnetite ($x < 0.2$) (Dunlop & Özdemir, 1997).

(iii) The remanence carriers must be single domain (SD) or pseudo-single domain (PSD) grains. It is widely accepted that multi domain (MD) grains give erroneous results because of the inequality of their blocking and unblocking temperatures and the influence of the thermal prehistory on pTRM intensity (Vinogradov & Markov, 1989). In order to determine the domain structure, we measured the hysteresis parameters using an alternative gradient force magnetometer at the Universidad Nacional Autonoma de Mexico. According to the criteria defined by Day et al. (1977) all the hysteresis parameters are in the PSD part of the plot (Fig. 5 and Table 2). However, a mixture of SD and MD grains could give the same result. Most samples are characterized by a very high median destructive field (Table 2) which is a further evidence of the presence of SD-PSD grains.

4.3 Preliminary selection of paleointensity data

The parameters used as criteria for a preliminary data selection are defined as follows, based on selection criteria commonly used for paleointensity experiments.

- (i) The number N of successive points on the linear segments chosen to calculate the paleointensity must be at least 4.
- (ii) The fraction of NRM destroyed on this segment must be greater than 1/3.
- (iii) The MAD calculated with the principal component calculated in the temperature interval used for paleointensity estimate must be less than 15° and the angle α between the vector average and this principal component also less than 15° (Selkin & Tauxe, 2000).
- (iv) The pTRM checks have to be positive, i.e. the deviation of pTRM quantified by the difference ratio (Selkin & Tauxe, 2000), which corresponds to the maximum difference between repeat pTRM steps normalized by the length of the selected NRM-pTRM segment, has to be less than 10% before and within the linear segment. Failure of a pTRM check is an indication of irreversible magnetic and/or chemical changes in the ferromagnetic minerals during the laboratory heating.

4.4 PTRM-tail test

In order to give us some indication about the domain states as a function of the temperature, we performed the pTRM-tail test that was first introduced by Bol'shakov & Shcherbakova (1979) and modified later by Shcherbakova et al. (2000). The principle of this test is as follows: if a sample is given a pTRM on an interval $[T_1, T_2]$ ($T_1 > T_2$), then is heated up to T_1 and cooled down in zero-field, the pTRM will be completely demagnetized only if the remanence carrier is single-domain. For pseudo-single-domain or multi-domain material, the pTRM will be completely demagnetized only after heating to a temperature higher than T_1 , this temperature reaching all the way to T_C for MD grains (Bol'shakov & Shcherbakova, 1979). Note that this test can only be applied to samples that do not alter chemically during heating. As discussed later, the Amsterdam samples are unusually stable, permitting wide application of this test.

The pTRM-tail test was carried out using a thermal vibrating magnetometer which allows the measurement of the magnetic remanence and the induced magnetization of a rock sample. The dimensions of the sample are 11 mm height and 10 mm diameter. The static residual field in the heating zone is less than 20 nT. It is possible to apply a direct field on the sample by sending a constant current to an inner coil placed between the detection coils and the heater. The two detection coils are connected in opposition. The sample is alternatively translated from the center of the first detection coil to the center of the other detection coil with a frequency of 13.7 Hz with 25.4 mm amplitude. The heater is powered with an alternating pulse width modulated current at a frequency of 3740 Hz. The output signal is directly applied to the current input of the lock-in amplifier Stanford Research SR830. After signal acquisition and calibration, we measure the magnetization moment versus temperature with a precision of $2 \times 10^{-8} \text{ Am}^2$ (with a time constant of 300 mS).

PTRM acquisitions were performed in air on sister samples (i.e., adjoining samples from the same paleomagnetic core), using a 100 μT field, in four different temperature intervals: $[300^\circ\text{C}, T_{room}]$, $[400^\circ\text{C}, 300^\circ\text{C}]$, $[500^\circ\text{C}, 400^\circ\text{C}]$ and $[550^\circ\text{C}, 500^\circ\text{C}]$. PTRMs were imparted "from above": the samples were first demagnetized by heating them in zero field to T_C ,

then a $100 \mu\text{T}$ is applied during the cooling down between the temperatures T_1 and T_2 , and pTRM(T_1, T_2) was measured at room temperature. Samples were subsequently heated again to T_1 , cooled down in zero field, and the tail of pTRM(T_1, T_2) measured at room temperature. Fig. 6 illustrates the succession of pTRM acquisitions and demagnetizations. We calculated the parameter A defined by

$$A(T_1, T_2) = \frac{\text{tail}[\text{pTRM}(T_1, T_2)]}{\text{pTRM}(T_1, T_2)} 100\% \quad (1)$$

as the relative intensity measured at room temperature of the pTRM tail remaining after heating to T_1 . According to the criteria defined by Shcherbakova et al. (2000), $A(T_1, T_2) < 4\%$ corresponds to SD, $4\% < A(T_1, T_2) < 15\%$ to PSD and $A(T_1, T_2) > 15\%$ to MD. Table 2 shows the values of $A(T_1, T_2)$ for the four temperature intervals used on the 17 remaining samples. All the samples have an MD response for pTRM's imparted in the intervals $[300^\circ\text{C}, T_r]$ and $[400^\circ\text{C}, 300^\circ\text{C}]$. However they all have a PSD response (except sample 669 which has an MD response) for the pTRM given in the interval $[500^\circ\text{C}, 400^\circ\text{C}]$, and PSD or SD response for a pTRM given in the interval $[550^\circ\text{C}, 500^\circ\text{C}]$. Fig. 7 illustrates typical MD and SD thermomagnetic behavior. Guided by these results we did not include any point on the Arai plot acquired before 400°C (500°C for sample 669) to calculate the paleointensity estimates.

4.5 Paleointensity results

Results are plotted as NRM lost as a function of pTRM gained on an Arai graph (Nagata et al., 1963). Examples of typical good samples are shown on Fig. 8 with associated orthogonal vector diagrams. Fourteen samples fulfilled all the criteria defined above and were then considered as yielding reliable results (Table 3). Most results have high quality factor (q) values (between 15 and 70) and the success rate of 50%, calculated on the whole collection, is very high and somewhat unusual for natural rocks.

Averaging four acceptable results, the flow am1 (excusional unit) gives a paleointensity of $24.6 \mu\text{T}$ and a Virtual Dipole Moment (VDM) of $3.7 \times 10^{22} \text{ Am}^2$ (Table 3). The flow am2 (excusional unit) gives an average paleointensity (using two results) of $24.0 \mu\text{T}$, corre-

sponding to a VDM of 3.4×10^{22} Am². The two normal flows (am3 and am4) give averages of $32.8 \mu\text{T}$ (using 5 values) and $46.9 \mu\text{T}$ (using 3 values), yielding VDM's of 6.2×10^{22} Am² and 7.7×10^{22} Am², respectively.

5 ^{40}Ar / ^{39}Ar AGE DETERMINATIONS

5.1 Analytical procedure

For each sample, 300 mg of whole rock fragments were carefully hand-picked under a binocular microscope from crushed 0.5 mm thick rock slabs. The samples were wrapped in Cu foil to form small packets as small as possible (11x11 mm.). These packets were stacked up to form a pile within which packets of flux monitors were inserted every 5 to 10 samples, according to the size of the samples. The stack, put in an irradiation can, was irradiated, with a Cd shield, for 1 hr at the McMaster University reactor (Hamilton, Canada) with a total flux of 1.3×10^{17} n.cm⁻². The irradiation standard was the Fish-Canyon sanidine (28.02 Ma; Renne et al. (1998)).

The sample arrangement allows monitoring of the flux gradient with a precision as low as ± 0.2 %. The step-heating experiment procedure was described in details by Ruffet et al. (1991). The mass spectrometer consists of a 120 M.A.S.S.E.[®] tube, a Bäur Signer[®] source and an SEV 217[®] electron-multiplier (total gain: 5×10^{12}) whereas the all metal extraction and purification lines include two SAES GP50W getters with St101[®] zirconium-aluminium alloy operating at 400°C and a -95°C cold trap. Samples were incrementally heated in a molybdenum crucible using a double vacuum high frequency furnace. The extraction segment of the line was pumped 3 minutes between each step.

Isotopic measurements are corrected for K and Ca isotopic interferences and mass discrimination. All errors are quoted at the 1σ level and do not include the errors on the $^{40}\text{Ar}^*/^{39}\text{Ar}_\text{K}$ ratio and age of the monitor. The error in the $^{40}\text{Ar}^*/^{39}\text{Ar}_\text{K}$ ratio of monitor is included in the isochron age error bars calculation.

5.2 $^{40}\text{Ar}^*/^{39}\text{Ar}_\text{K}$ results

The very low K- and rather high Ca-contents of the analyzed samples and their very young apparent age were unfavorable parameters to produce high quality analyses and to obtain unambiguous results. The classical calculation method using an $^{40}\text{Ar}/^{36}\text{Ar}$ atmospheric ratio measured on an air aliquot resulted in zero apparent ages for successive degassing steps, probably as a result of an inadequate procedure for determining this ratio. The very high ratio of the measured atmospheric to the radiogenic ^{40}Ar favors use of isochron calculation (correlation method: $^{36}\text{Ar}/^{40}\text{Ar}$ versus $^{39}\text{Ar}^*/^{40}\text{Ar}_\text{K}$; e.g. Turner (1971); Roddick et al. (1980); Hanes et al. (1985)). This method does not require "a priori" knowledge of the measured $^{40}\text{Ar}/^{36}\text{Ar}$ atmospheric ratio. Two argon components can be identified using this calculation method: the first one, related to the atmosphere, is usually weakly linked to the mineral; the other one, supplied by radioactive decay of ^{40}Ar , is trapped in minerals structures. The aim of degassing by steps is to separate, at least partly, these two components, which allows a mixing line to be defined, the isochron. In whole rock analysis, a meaningful isochron must be calculated on a degassing segment which corresponds to the degassing of a specific mineral phase.

All analyzed samples display rather constant $\text{CaO}/\text{K}_2\text{O}$ calculated ratios in the intermediate temperature range, around 11 ($\text{CaO}/\text{K}_2\text{O} = {^{37}\text{Ar}_{\text{Ca}}}/{^{39}\text{Ar}_\text{K}} \times 2.179$; Deckart et al. (1997)), which suggest degassing of a homogeneous phase, probably plagioclase as observed in thin sections. Very young calculated isochron ages (Fig. 9), concordant at the 2σ level, are obtained from the corresponding degassing steps (Table 4). They suggest that the two sampled lava flows with intermediate directions could be as young as 20-25 ka and the lava flow (am3) with the normal direction slightly older at ca 45 ka.

6 DISCUSSION

6.1 Reliability of paleointensity estimates

The determination of absolute paleointensity by the Thellier method imposes many constraints on rock magnetic properties which are often not respected in natural rocks. The failure rate is usually around 70-90% (Perrin, 1998). We obtained results of very good technical quality for 50% of the samples in this study. Nevertheless a recent study carried out on historical lava flows from Mount Etna showed that samples which fulfilled all the reliability criteria imposed by the authors could yield a paleointensity exceeding the real field paleomagnitude by as much as 25% (Calvo et al., 2002). It should never be forgotten that measurements of paleointensity are only estimates. Therefore we wish to discuss further the reliability of the paleointensity measurements performed in the present study.

First, we can make sure that the part of NRM used must be a TRM. We compared continuous thermal demagnetization curves of NRM and artificial (total) TRM of sister samples measured using the thermal vibrating magnetometer. The artificial TRM was imparted in the direction of the NRM. Samples have to be drilled in the direction of the NRM; therefore we did this test only for 3 samples because we did not have enough material. A result is shown in Fig. 10. The remarkable similarity between the thermal demagnetization of the NRM and of the artificial TRM suggests that the NRM is a TRM and confirms the thermal stability of Amsterdam lava.

Thermal stability can be further tested independently by comparing the laboratory Koenigsberger ratios before and after heating. The ratio before heating is calculated according to the formula:

$$Q_L = \frac{M_{nrm}}{k_a \cdot H_a}, \quad (2)$$

where M_{nrm} is the natural remanent magnetization, k_a is the bulk magnetic susceptibility measured before paleointensity experiments and H_a is the ancient field obtained from the paleointensity experiments. The ratio after heating is defined by:

$$Q'_L = \frac{M_{trm}}{k_b \cdot H_{lab}}, \quad (3)$$

where M_{trm} is the total TRM obtained by extrapolation of the data corresponding to the highest temperatures on the Arai plot, k_b is the bulk magnetic susceptibility obtained after heating and H_{lab} is the laboratory field. We observed that the two Koenigsberger ratios have similar values for the samples that gave reliable paleointensity results (Table 5). This suggests that these samples are thermally stable.

The hysteresis parameters (Fig. 5 and Table 2) show that all the samples have a behavior characteristic of PSD grains. In natural samples, this is usually interpreted as the indication of a mixture of SD-PSD and MD grains. We found that one of the advantages of performing the pTRM-tail-test over measuring hysteresis parameters is to allow us to discriminate between MD, PSD and SD thermomagnetic behavior. This test qualifies directly the TRM behavior, contrary to the hysteresis curves which make tests on remanent or induced magnetizations of isothermal origin. Moreover, it seems that measurement of hysteresis parameters as a function of temperature sometimes does not allow detection of changes in domain structure with heating (Carvallo & Dunlop, 2001). We note in Fig. 5 that the accepted samples (black dots) generally have higher Mrs/Ms than the rejected samples (white dots). Thus, on average the better samples for paleointensity are a little smaller in effective magnetic grain size.

6.2 pTRM-tail-test : A new tool for paleointensity experiments ?

The main methodological originality of the present study is the use of pTRM-tail tests to select the most suitable portion of the NRM-TRM diagrams. Many authors (e.g., Shcherbakova et al. (2000)) have suggested that recognizing the multidomain component in the paleointensity experiment is critical for the exactitude of the final result. The presence of multidomain grains will invalidate the Thellier method if the unblocking temperature does not equal the blocking temperature any more. Using the part of the Arai plot derived from multidomain behavior can thus lead to large errors in the paleointensity measurement. For example, Shcherbakov & Shcherbakova (2001) showed that, if one were to ignore the continuous curvature and fit a line to low temperature data points of synthetic, purely MD samples,

one could overestimate the true value by as much as 60%. For the majority of the samples that we tested, the relative tails $A(T_1, T_2)$ are very large when pTRM is imparted at low-temperatures (300°C - T_{room} and 400°C - 300°C), but become smaller and smaller for higher temperature intervals Table 2, which led us to reject all points acquired below 400°C in calculating the paleointensities. Shcherbakova et al. (2000) as well as Shcherbakov & Shcherbakova (2001) also observed a diminution of the pTRM tail with increasing temperature intervals, using both natural and synthetic samples.

In our case, this behavior could be explained in several ways.

(i) Our natural samples are composed of a mixture of grains having different sizes. It is possible that the MD part of the remanence carriers have lower Curie temperature, whereas PSD and SD grains carry the high-temperature remanence (Dunlop & Özdemir, 2001). A simplified explanation of what is observed with the variations of A parameters is that mainly MD grains are magnetized when they are given a low temperature pTRM ($< 400^{\circ}\text{C}$), yielding high A values. For high temperature pTRMs ($> 400^{\circ}\text{C}$), mainly PSD/SD grains are magnetized and give very small tails. Another indication of the presence of MD material can be extracted from the pTRM acquisition curve: when the field is switched off during the cooling, the magnetic moment drops because of the presence of induced magnetization which is more important for MD than SD grains. For example, the pTRM (500°C , 400°C) acquired by sample 680 has a large tail (60%), and the magnetic moment drops of about 50% when the field is switched off at 400°C (Fig. 7). But for sample 675, which has a tail for the pTRM(550°C , 500°C) of only 2.2%, the drop when the field is switched off is also much smaller (about 10% of the remanence acquired at this temperature). This is a general trend observed for the ensemble of the pTRM acquisitions-demagnetizations (Fig. 11), although a more precise correlation is difficult to establish.

(ii) Alternatively, one could argue that for the samples having high Curie points, the high values of the low temperature pTRM tails might be only due to the fact that the pTRMs acquired in these intervals are actually very low. The difference between the magnetic moment measured after acquisition of a small pTRM and the magnetic moment measured after

its demagnetization might then not be significant of any physical process but only reflect an artifact created by the accuracy of the measurement. However, the ranges of magnetization measured are in most cases well above the sensitivity of the vibrating magnetometer, so we can be quite confident that the measured values of A in Table 2 are physically meaningful.

From a practical point of view, the pTRM-tail test was not critical for these Amsterdam basalt samples. Before knowing the $A(T_1, T_2)$ values, we selected samples and temperature steps for estimating paleointensity from our Thellier data using conventional criteria –*i.e.*, essentially items i-iv described above in section 4.3. The flow-mean values thus obtained do not differ significantly from those obtained by adding further data selection according to the pTRM-tail test. In retrospect, this is not unexpected because, the selected samples have 57 to 91% (on average 81%) of their TRM remaining after thermal demagnetization to 400°C. Thus, the pTRM tails of the low-temperature points are too small to have an appreciable effect on the slope of the best-fit lines of the Arai diagrams, that is, on the paleointensity estimate. More difficult to understand is the low-temperature slope of sample 680 which have more than 30% of its remanence below 400°C. Its multidomain-size pTRM tails would lead one to expect slope corresponding to large overestimated of paleointensity, but actually that for 680 is too low by 33%. At this time we have no explanation for the departure of this sample from the behavior expected for multidomain grains (Dunlop & Özdemir, 2001; Shcherbakov & Shcherbakova, 2001).

6.3 Implication for the excursion field characteristics

Studies carried out on absolute paleointensity during the Brunhes period show generally a decrease of the VDM value when the colatitude of the VGP increases. This trend is illustrated in Fig. 12a in which we gathered Brunhes VDMs from the paleointensity database PINT2000 using as the unique selection criteria the Thellier paleointensity method. The VDM obtained in the present study, showing approximately a ratio of 2 between the normal and the excursion field, fit well in this general tendency. In Fig. 12b, we have randomly generated 500 VDMs from the statistical model of Camps & Prévot (1996) for fluctuations

in the geomagnetic field, using the model parameters proposed for the Icelandic data set. In this model, the local field vector is the sum of two independent sets of vectors: a normally distributed axial dipole component plus an isotropic set of vectors with a Maxwellian distribution that simulates secular variation. It is worth pointing out that the trend in the experimental VDMs for the Brunhes period is very well reproduced in this statistical model. We do note that this simulation also predicts some outliers data – high VDMs corresponding to excursion VGP – as it sometimes observed in the Brunhes experimental data set (Fig. 12a) and as has been also recently reported for a mid Miocene excursion recorded in Canary Island lavas (Leonhardt et al., 2000).

Abnormal VGPs from the Amsterdam excursion tend to group over the Caribbean Sea (Fig. 13). The question of whether this cluster represents a long-lived transitional state of the field or is an artifact due to a rapid extrusion of successive lavas must be addressed. First, Watkins & Nougier (1973) concluded from geological field observations that Amsterdam excursion seems to correspond to two successive departures of the VGPs from the present geographic pole which recorded very similar VGP locations. They argued that one of the excursion flow (their flow 24) belongs to the old volcanic episode whereas all the other excursion flows (their flows 13,17-19), although they yield a similar abnormal direction, are part of a more recent volcanic phase. We know from experience that stratigraphic correlations are often speculative in volcanic area, hence we find their argument quite weak. However we have no reason to rule out their conclusion since we did not carry out a field analysis. Next, we note that one of the excursion VGP from the Laschamp event (Fig. 13b) has also a location within the Amsterdam cluster. Finally, we point out that Camps et al. (2001) have described a Plio-Pleistocene normal-transitional-normal excursion recorded in lava flows from Possession Island, a volcanic island located in the southern India ocean 2300 km southwestward from Amsterdam. Interestingly, this excursion is characterized by a clustering of transitional VGPs also located in the vicinity of the Caribbean Sea (Fig. 13c). Although this excursion is not radiometrically dated, we are certain from geological considerations that it is older than the Amsterdam excursion. Thus, the transitional field of at

least two distinct excursions would have revisited the same VGP location. These observations suggest that the Amsterdam excursion cluster may represents a recurring preferred location for transitional VGPs like that was previously proposed (Hoffman, 1992).

At present, the Ar/Ar isotopic ages suggest that the Amsterdam excursion corresponds to a late Pleistocene excursion. During this period, two geomagnetic events are described in the literature. It concerns the Mono Lake excursion, documented in several lacustrine sedimentary sections from the western USA, which is dated to ≈ 28 ^{14}C ka (Liddicoat, 1992), and the Laschamp excursion, described for the first time in lava flows from La chaine des Puys, Massif Central France, and dated to ≈ 42 ka (see Kent et al. (2002) for a review). If evidences for the Laschamp excursion are found in numerous deep-sea sediment records, this is not the case for the Mono Lake which is only described jointly with Laschamp from high deposition rate sediments in the North Atlantic (Nowaczyk & Antonow, 1997; Laj et al., 2000). At the present time, the existence of two geomagnetic excursions in the late Pleistocene is directly questioned by Kent et al. (2002). Using new ^{14}C dates on carbonates and $^{40}\text{Ar}/^{39}\text{Ar}$ sanidine dates on ash layers, they concluded that Mono Lake excursion at Wilson Creek should be regarded as a record of the Laschamp excursion. Unfortunately, the large error bars associated with ours ages estimate for the Amsterdam excursion do not allow to bring insight into this debate. We point out here that our preferred hypothesis, taking into account the age of 26 ± 15 and 18 ± 9 ka obtained for Amsterdam excursion flows, is to correlate this excursion with a geomagnetic event younger than 30 Ka which could correspond to Mono Lake if we consider the former age estimate of 28 Ka (Liddicoat, 1992). This conclusion requires however a further confirmation with a more accurate age control, but if it is true, Amsterdam excursion would represent firm evidence for a global occurrence of Mono Lake excursion. Finally, it is interesting to point out that the original record of Mono Lake excursion at Wilson Creek (Liddicoat & Coe, 1979) shows, as the Amsterdam excursion seems to do, two successive excursion loops (Fig. 13a).

7 CONCLUSIONS

- (i) We have identified an excursion of the geomagnetic field in the late Pleistocene recorded in volcanic rocks from Amsterdam Island, Indian Ocean. Good quality alternating field demagnetization results show that two flows have excursion polarities with VGP latitudes of 15.2° and 21.2° , and two flows have normal polarities (VGP latitudes are 85.5° and 77.4°).
- (ii) $^{40}\text{Ar}/^{39}\text{Ar}$ dating did not enable us to precisely specify which excursion we identified. Mono Lake is the most likely, but the large error bars in the final dates do not exclude the possibility for these rocks to have recorded the Laschamp excursion. Indeed, some authors believe the two excursions are the same (Kent et al., 2002)
- (iii) High-quality paleointensity determinations show low VDM values for the excursion flows ($3.7 \times 10^{22} \text{ Am}^2$ and $3.4 \times 10^{22} \text{ Am}^2$), whereas normal flows have VDMs close to the present-day VDM ($6.2 \times 10^{22} \text{ Am}^2$ and $7.7 \times 10^{22} \text{ Am}^2$). These low values are in agreement with other VDMs determinations during excursions in the Brunhes period and corroborates the fact that the VDM decreases when the colatitude of VGP increases.
- (iv) For the first time, pTRM-tail-tests from above were used as a selection criteria for the paleointensity determinations. We found that most of our samples exhibit a tail characteristic of MD material for pTRMs given at low temperature and SD-like for high-temperature pTRMs. Therefore we rejected measurements acquired at low-temperature ($> 400^\circ\text{C}$) for the best-fit on the Arai plots.

ACKNOWLEDGMENTS

We are grateful to the “Institut Polaire Paul Emile Victor” for providing all transport facilities and for the support of this project. Special thanks to A. Lamalle and all our field friends. We thank M. Prévot, A. Muxworthy, R. Coe, Ö. Özdemir and D.J. Dunlop for valuable discussions, A. Goguitchaichvili for carrying out the hysteresis measurements, and Anne Delplanque for assistance with computer drawing. The comments of S. Bogue, C. Langereis and an anonymous reviewer are appreciated. This work was supported by CNRS-INSU programme intérieur Terre.

REFERENCES

Audunsson, H. & Levi, S., 1997. Geomagnetic fluctuations during a polarity transition, *J. Geophys. Res.*, **102**(B9), 20259–20268.

Bol'shakov, A. & Shcherbakova, V., 1979. A thermomagnetic criterion for determining the domain structure of ferrimagnetics, *Izv. Acad. Sci. USSR Phys. Solid Earth*, **15**, 111–117.

Calvo, M., Prévot, M., Perrin, M., & Riisager, J., 2002. Investigating the reasons for the failure of paleointensity experiments: A study on historical lava flows from mt. etna (italy), *Geophys. J. Int.*, p. Under Press.

Camps, P. & Prévot, M., 1996. A statistical model of the fluctuations in the geomagnetic field from paleosecular variation to reversal, *Sciences*, **273**, 776–779.

Camps, P., Henry, B., Prévot, M., & Faynot, L., 2001. Geomagnetic paleosecular variation recorded in plio-pleistocene volcanic rocks from Possession Island (Crozet Archipelago, southern Indian Ocean, *J. Geophys. Res.*, **106**(B2), 1961–1972.

Carvallo, C. & Dunlop, D., 2001. Archeomagnetism of potsherds from Grand Banks, Ontario: a test of low paleointensities in Ontario around A.D.1000., *Earth Planet. Sci. Lett.*, **186**, 437–450.

Chauvin, A., Duncan, R., Bonhommet, N., & Levi, S., 1989. Paleointensity of the Earth's magnetic field and K-Ar dating of the Louchedière flow (Central France), new evidence for the Laschamps excursion, *Geophys. Res. Lett.*, **16**, 1189–1192.

Coe, R., Grommé, C., & Mankinen, E., 1978. Geomagnetic paleointensities from radiocarbon-dated lava flows on Hawaii and the question of the Pacific nondipole low, *J. Geophys. Res.*, **83**, 1740–1756.

Day, M., Fuller, M., & Schmidt, V., 1977. Hysteresis properties of titanomagnetites: grain size and compositional dependance., *Phys. Earth Planet. Int.*, **13**, 267–267.

Deckart, K., Féraud, G., & Bertrand, H., 1997. Age of Jurassic continental tholeiites of French Guyana, Surinam and Guinea; implications for the initial opening of the central Atlantic Ocean, *Earth Planet. Sci. Lett.*, **150**(3-4), 205–220.

Dunlop, D. & Özdemir, O., 1997. *Rock magnetism: Fundamentals and frontiers*, Cambridge Univ. Press, New-York, 573 pp.

Dunlop, D. & Özdemir, O., 2001. Beyond Néel's theories: thermal demagnetization of narrow-band partial thermoremanent magnetizations., *Phys. Earth Planet. Int.*, **126**(1-2), 43–57.

Graham, D., Johnson, K., Douglas Priebe, L., & Lupton, J., 1999. Hotspot-ridge interaction along the Southeast Indian Ridge near Amsterdam and St Paul islands: helium isotope evidence, *Earth Planet. Sci. Lett.*, **167**, 297–310.

Gubbins, D., 1999. The distinction between geomagnetic excursions and reversals, *Geophys. J. Int.*, **137**, F1–F3.

Gunn, B., Abranson, C., Nougier, J., Watkins, N., & Hajash, A., 1971. Amsterdam island, an isolated volcano in the Southern Indian Ocean, *Contr. Mineral. and Petrol.*, **32**, 79–92.

Guyodo, Y. & Valet, J., 1999. Global changes in intensity of the Earth's magnetic field during the past 800 kyr, *Nature*, **399**, 249–252.

Hanes, J., York, D., & Hall, C., 1985. An $^{40}\text{Ar}/^{39}\text{Ar}$ geochronological and electron microprobe investigation of an Archean pyroxenite and its bearing on ancient atmospheric compositions, *Can. J. Earth Sci.*, **22**, 947–958.

Hoffman, K., 1981. Palaeomagnetic excursions, aborted reversals and transitional fields, *Nature*, **294**, 67–69.

Hoffman, K., 1992. Dipolar reversal states of the geomagnetic field and core-mantle dynamics, *Nature*, **359**, 789–794.

Johnson, K., Graham, D., Rubin, K., Nicolaysen, K., Scheirer, D., Forsyth, D. W., Baker, E. T., & Douglas-Priebe, L. M., 2000. Boomerang Seamount; the active expression of the Amsterdam-St. Paul Hotspot, Southeast Indian Ridge, *Earth and Planet. Sci. Lett.*, **183**, 245–259.

Kent, D., Hemming, S., & Turrin, B., 2002. Laschamp excursion at Mono Lake?, *Earth Planet. Sci. Lett.*, **197**, 151–164.

Kirschvink, J., 1980. The least-squares line and plane and the analysis of paleomagnetic data, *Geophys. J. R. astr. Soc.*, **62**, 699–718.

Laj, C., Kissel, C., Mazaud, A., Channell, J., & Beer, J., 2000. North Atlantic palaeointensity stack since 75 ka (napis-75) and the duration of the Laschamp event, *Phil. Trans. R. Soc. Lond. A*, **358**, 1009–1025.

Langereis, C., Dekkers, M., de Lange, G., Paterne, M., & van Santvoort, P., 1997. Magnetostratigraphy and astronomical calibration of the last 1.1 Myr from an eastern Mediterranean piston core and dating of short events in the Bruhnes, *Geophys. J. Int.*, **129**, 75–94.

Leonhardt, R., Hufenbecher, F., Heider, F., & Soffel, H., 2000. High absolute paleointensity during a mid Miocene excursion of the Earth's magnetic field, *Earth Planet. Sci. Lett.*, **184**, 141–154.

Levi, S. & Karlin, R., 1989. A sixty thousand year paleomagnetic record from Gulf of California sediments: secular variation, late Quaternary excursions and geomagnetic implications, *Earth Planet. Sci. Lett.*, **92**, 219–233.

Levi, S., Audunaaon, H., Duncan, R., Kristjansson, L., Gillot, P., & Jacobsson, S., 1990. Late Pleistocene geomagnetic excursion in Icelandic lavas: confirmation of the Laschamps excursion, *Earth Planet. Sci. Lett.*, **96**, 443–457.

Liddicoat, J., 1992. Mono Lake excursion in Mono Basin, California, and at Carson Sink and Pyramid Lake, Nevada, *Geophys. J. Int.*, **108**, 442–452.

Liddicoat, J., 1996. Mono Lake excursion in the Lahontan Basin, Nevada, *Geophys. J. Int.*, **125**,

630–635.

Liddicoat, J. & Coe, R., 1979. Mono Lake geomagnetic excursion, *J. Geophys. Res.*, **1984**, 261–271.

Nagata, T., Arai, Y., & Momose, K., 1963. Secular variation of the geomagnetic total force during the last 5,000 years, *J. Geophys. Res.*, **68**, 5277–5282.

Nowaczyk, N. & Antonow, M., 1997. High-resolution magnetostratigraphy of four sediment cores from the Greenland Sea – I. Identification of the Mono Lake excursion, Laschamp and Biwa I/Jamaica geomagnetic polarity events, *Geophys. J. Int.*, **131**, 310–324.

Perrin, M., 1998. Paleointensity determination, magnetic domain structure, and selection criteria, *J. Geophys. Res.*, **103**, 30591–30600.

Prévot, M., Mankinen, E., Grommé, C., & Lecaille, A., 1983. High paleointensities of the geomagnetic field from thermomagnetic study on rift valley pillow basalts from Mid-Atlantic Ridge, *J. Geophys. Res.*, **88**, 2316–2326.

Quidelleur, X., Gillot, P., Carlut, J., & Courtillot, V., 1999. Link between excursions and paleointensity inferred from abnormal field directions recorded at La Palma around 600 ka, *Earth Planet. Sci. Lett.*, **168**, 233–242.

Renne, P., Swisher, C., Deino, A., Karner, D., Owens, T., & DePaolo, D., 1998. Intercalibration of standards, absolute ages and uncertainties in $^{40}\text{Ar}/^{39}\text{Ar}$ dating, *Chem. Geol.*, **154**, 117–152.

Roddick, J., Cliff, R., & Rex, D., 1980. The evolution of excess argon in alpine biotites- A $^{40}\text{Ar}/^{39}\text{Ar}$ analysis, *Earth Planet Sci. Lett.*, **48**, 185–208.

Roperch, P., Bonhommet, N., & Levi, S., 1988. Paleointensity of the Earth's magnetic field during the Laschamps excursion and its geomagnetic implications, *Earth Planet. Sci. Lett.*, **88**, 209–219.

Royer, J. & Schlich, R., 1988. Southeast Indian Ridge between the Rodriguez triple junction and the Amsterdam and Saint Paul Islands: detailed kinematics for the past 20 m.y., *J. Geophys. Res.*, **93**, 13524–13550.

Ruffet, G., Féraud, G., & Amouric, M., 1991. Comparison of $^{40}\text{Ar}/^{39}\text{Ar}$ conventional and laser dating biotites from the North Trégor Batholith, *Geochim. et Cosmochim. Acta*, **55**, 1675–1688.

Schnepp, E. & Hradetzky, H., 1994. Combined paleointensity and $^{40}\text{Ar}/^{39}\text{Ar}$ age spectrum data from volcanic rocks of the West Eifel field (Germany): evidence for an early Brunhes geomagnetic excursion, *J. Geophys. Res.*, **99**(B5), 9061–9076.

Selkin, P. & Tauxe, L., 2000. Long term variations in palaeointensity, *Phil. Mag.*, **358**(1768), 1065–1088.

Shcherbakov, V. & Shcherbakova, V., 2001. On the suitability of the Thellier method of paleointensity determinations on pseudo-single-domain and multidomain grains., *Geophys. J. Int.*, **146**,

20–30.

Shcherbakova, V., Shcherbakov, V., & Heider, F., 2000. Properties of partial thermoremanent magnetization in pseudosingle domain and multidomain magnetite grains, *J. Geophys. Res.*, **105**, 77767–781.

Small, C., 1995. Observation of ridge-hotspot interactions in the Southern Ocean, *J. Geophys. Res.*, **100**(B9), 17931–17946.

Tauxe, L., 1998. *Paleomagnetic Principles and Practice*, Kluwer, Dordrecht.

Thellier, E. & Thellier, O., 1944. Recherches géomagnétiques sur des coulées volcaniques d'Auvergne, *Ann. Geophys.*, **1**, 37–52.

Thellier, E. & Thellier, O., 1959. Sur l'intensité du champ magnétique terrestre dans le passé historique et géologique, *Ann. Geophys.*, **15**, 285–376.

Turner, G., 1971. $^{40}\text{Ar}/^{39}\text{Ar}$ ages from the lunar Maria, *Earth Planet. Sci. Lett.*, **11**, 169–191.

Vinogradov, Y. & Markov, G., 1989. *On the effect of low temperature heating on the magnetic state of multi-domain magnetite- Investigations in Rockmagnetism and Paleomagnetism*, pp. 31–39, Institute of Physics of the Earth, Moscow.

Watkins, N. & Nougier, J., 1973. Excursions and secular variations of the Brunhes epoch geomagnetic field in the Indian ocean region, *J. Geophys. Res.*, **78**(26), 6060–6068.

Zhu, R., Pan, Y., & Coe, R., 2000. Paleointensity studies of a lava succession from Jilin Province, northeastern China: Evidence for the Blake event, *J. Geophys. Res.*, **105**, 8305–8317.

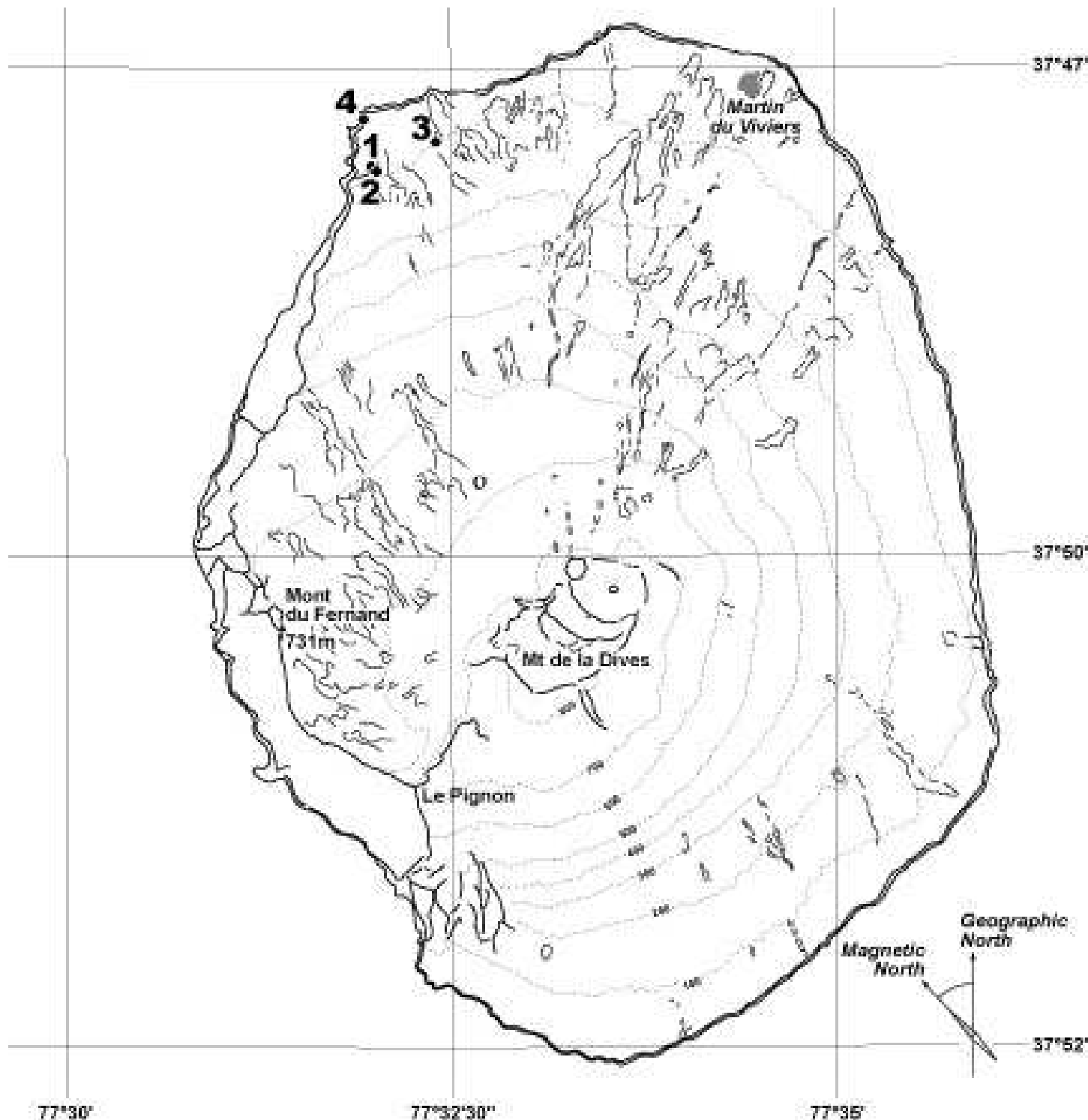


Figure 1. Location of the four sampled flows on a topographic map of Amsterdam Island

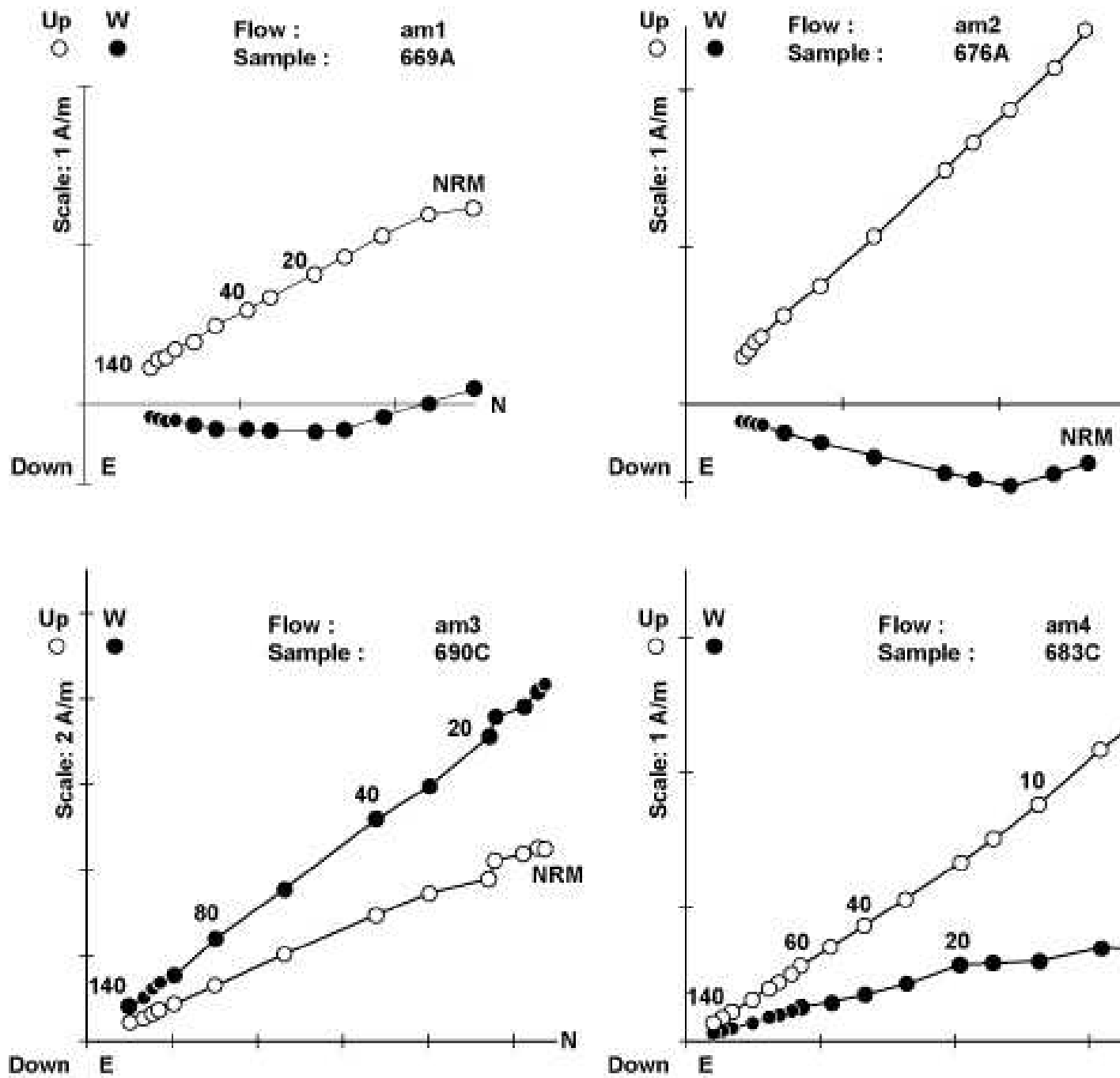


Figure 2. Orthogonal projections of alternating-field demagnetization for one pilot sample from each lava flow. Solid (open) symbols represent projection into horizontal (vertical) planes.

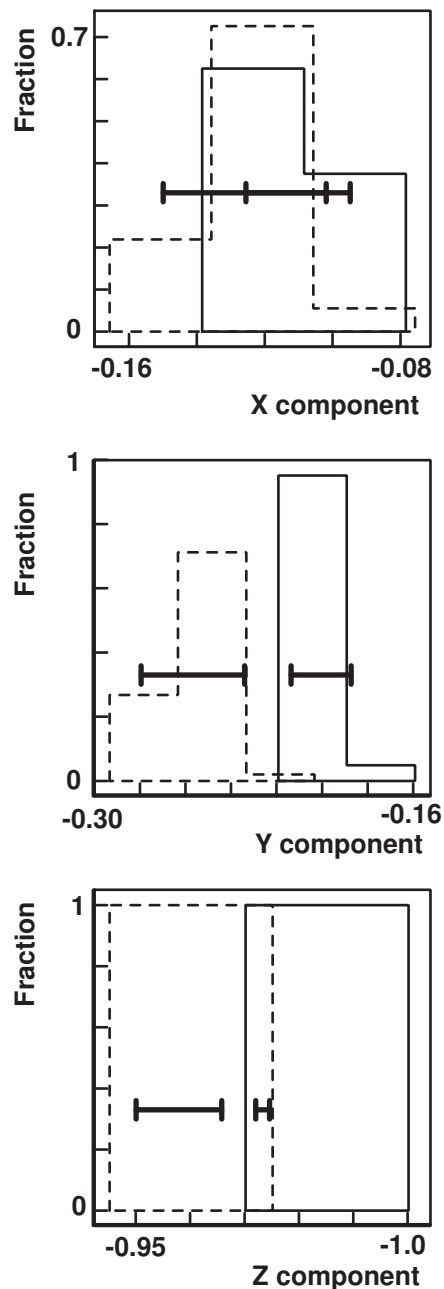


Figure 3. The bootstrap test for a common mean direction for flows am1 and am2 (Tauxe, 1998) illustrated by the histograms of the cartesian coordinates of the bootstrapped means for flows am1 (solid line) and am2 (dashed line). Because the 95% confidence intervals for Y and Z components do not overlap, we assume that the two lava flows have a significantly different mean direction.

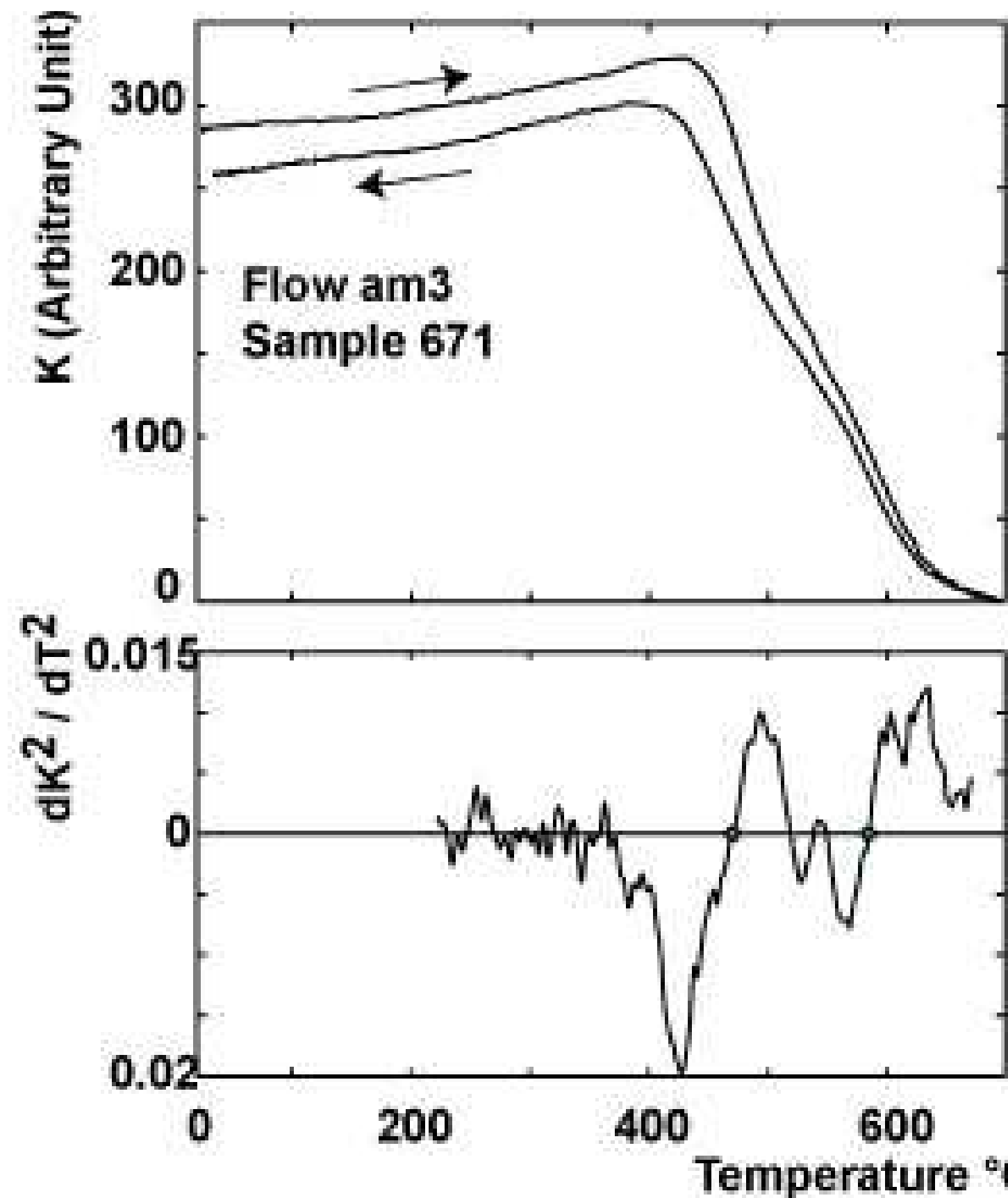


Figure 4. Example of thermal variation of weak field magnetic susceptibility K (measured in induction B equal to $100\mu\text{T}$) against temperature $T(\text{°C})$ showing a good reversibility and second

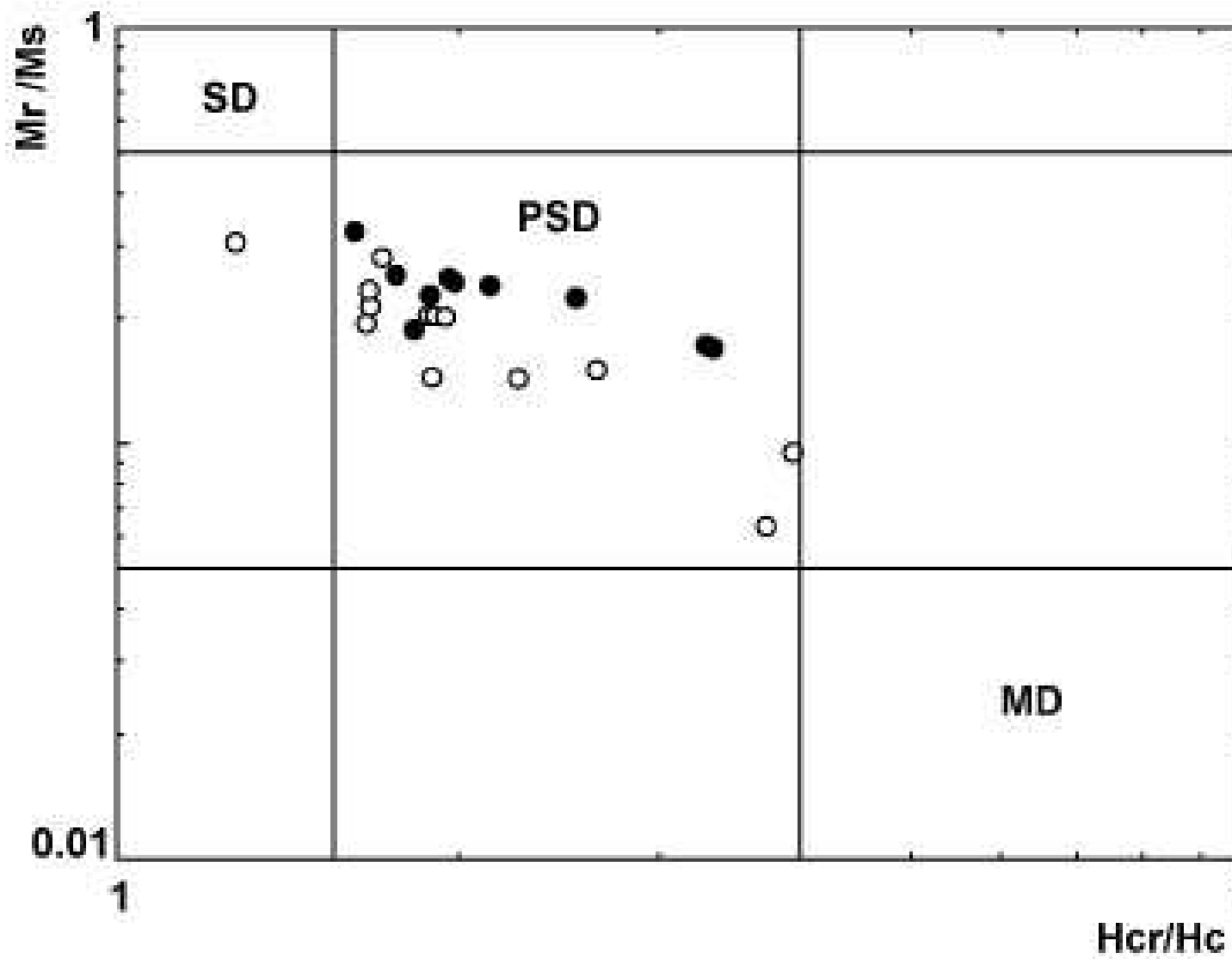


Figure 5. Hysteresis parameters ratio measured at room temperature plotted on a log-log scale. Solid (open) symbols correspond to accepted (rejected) samples for paleointensity experiments on the basis of selection and reliability criteria discussed in the text.

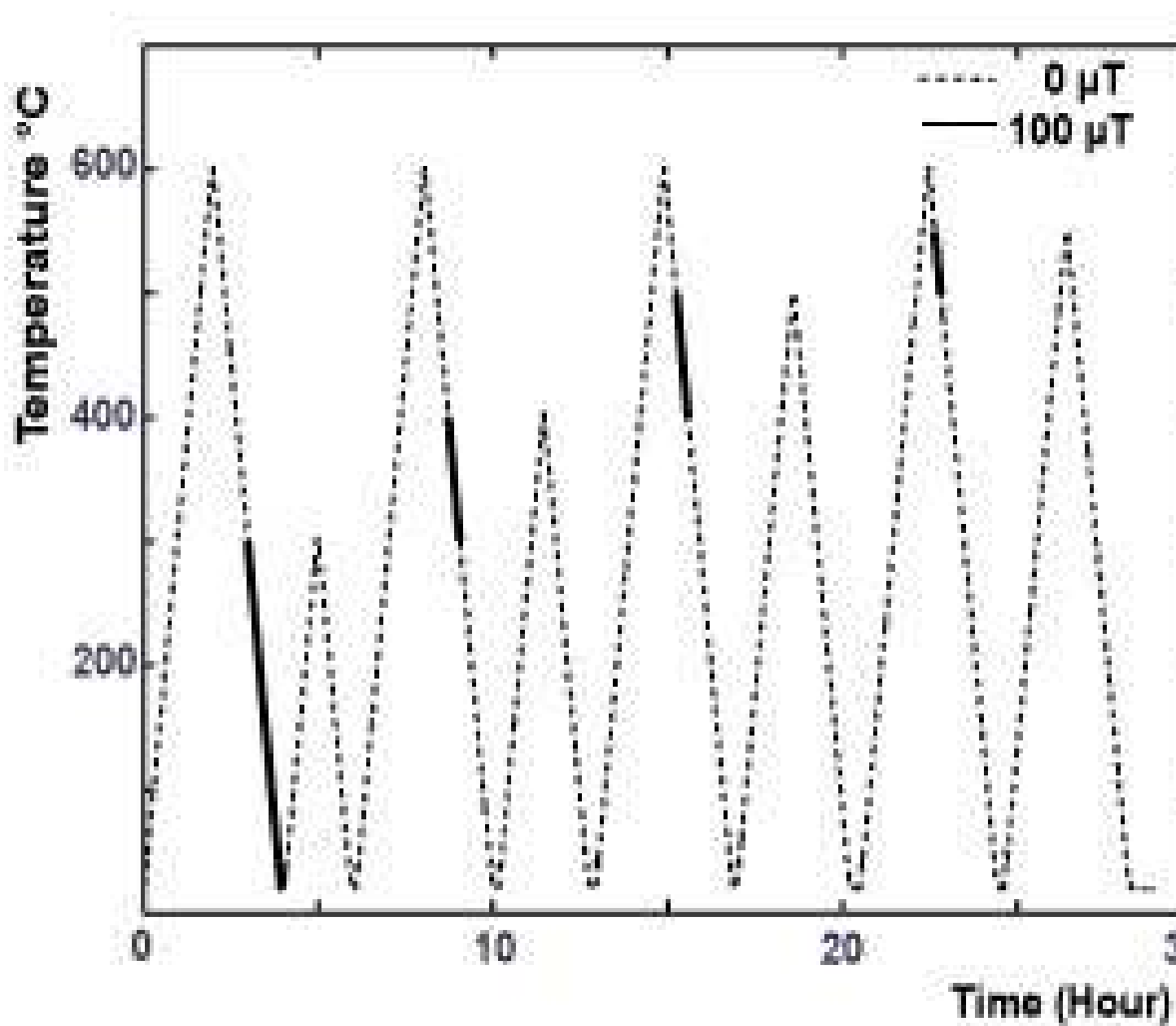


Figure 6. Temperature as a function of time for a sample heated and cooled at a constant rate of $5^\circ/\text{mn}$. The curve shows the succession of pTRM acquisitions in an applied field of $100 \mu\text{T}$ (solid line) during cooling and demagnetizations (dashed line) carried out during the pTRM-tail test. Parameter A is calculated as the ratio of the intensity of the tail of pTRM normalized by the original pTRM, both measured at room temperature

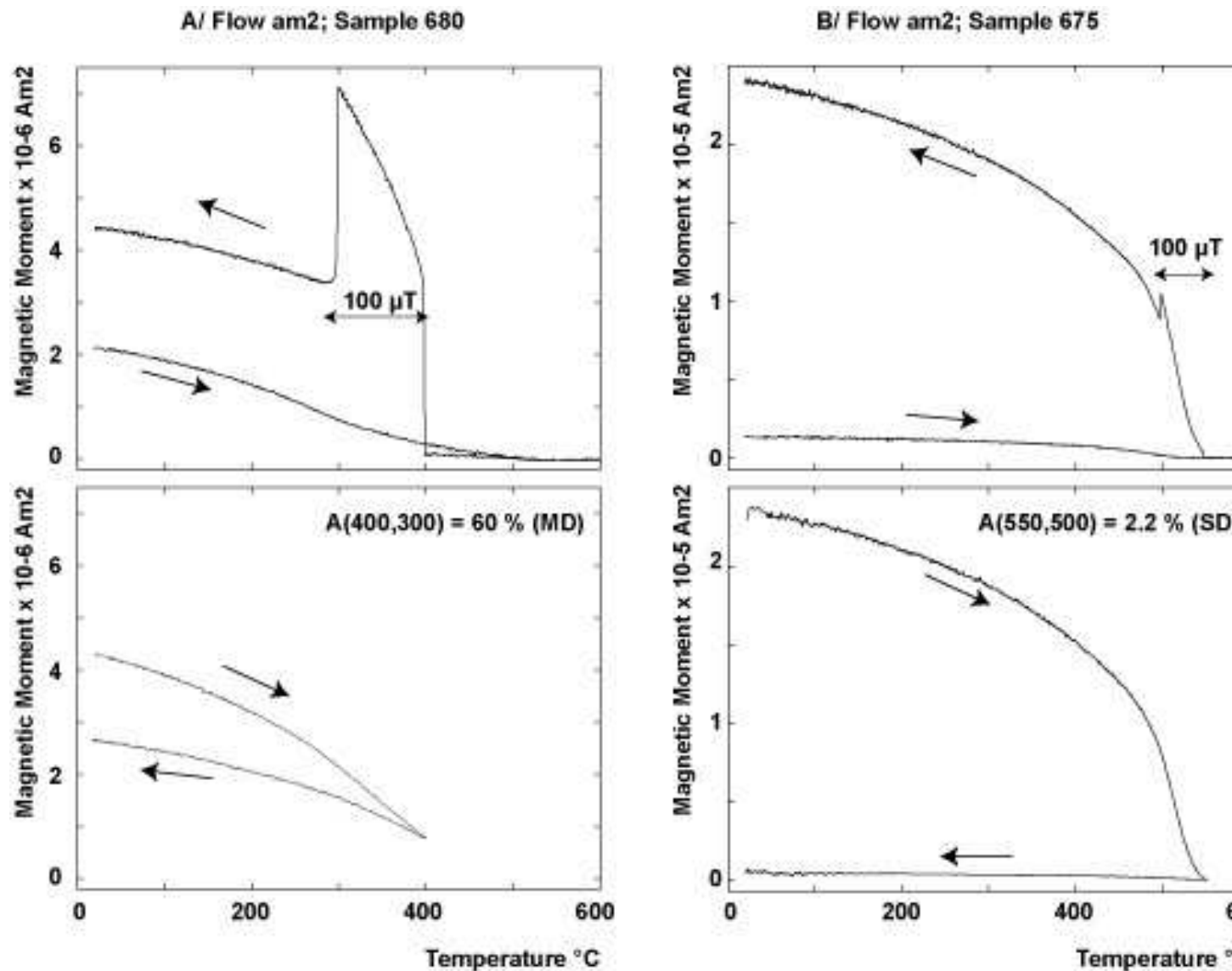
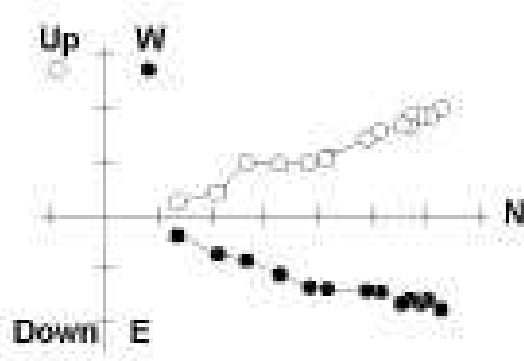
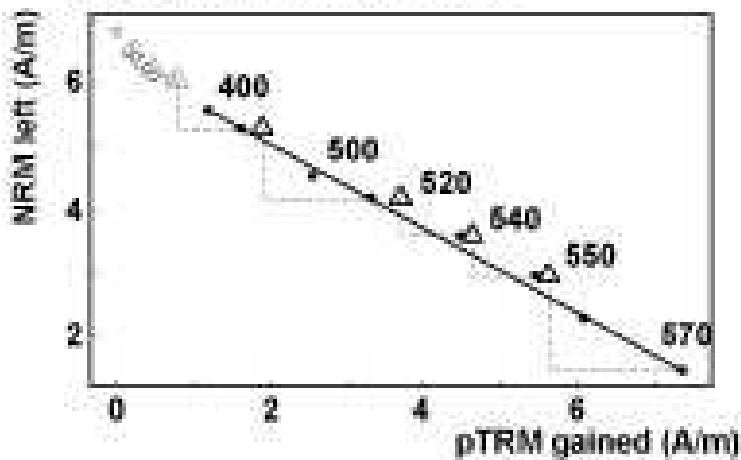
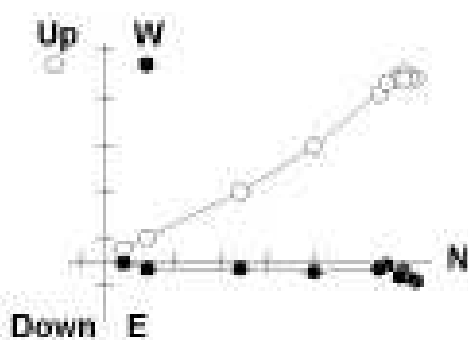
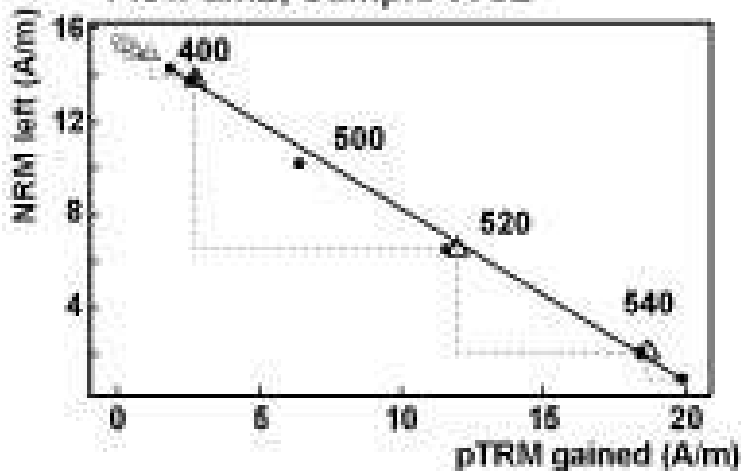


Figure 7. Thermomagnetic curves acquired during pTRM acquisition (top) and pTRM demagnetization (bottom). In example A the pTRM is imparted on the interval (400°C-300°C). Subsequent demagnetization to 400°C leaves an important tail. In example B, the pTRM is imparted on the interval (550°-500°C) and is almost completely demagnetized after heating back to 550°C.

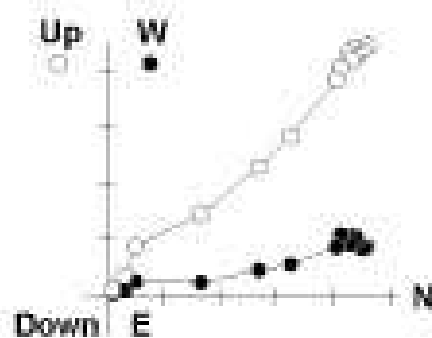
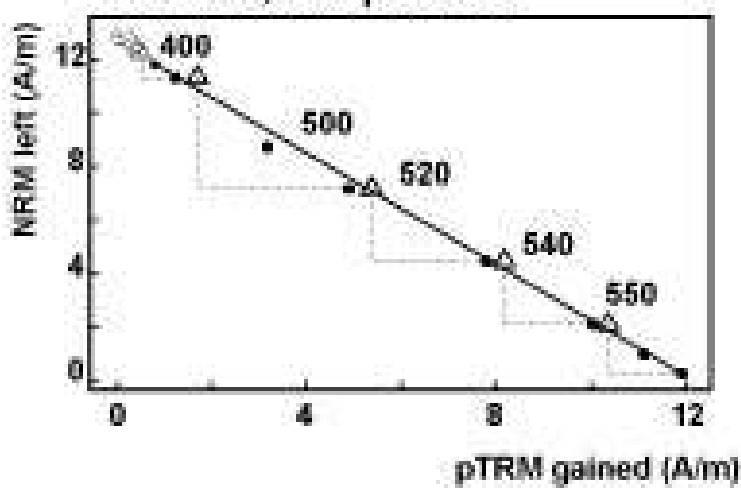
Flow am1; Sample 670D



Flow am2; Sample 675E



Flow am3; Sample 695B



Flow am4; Sample 686E



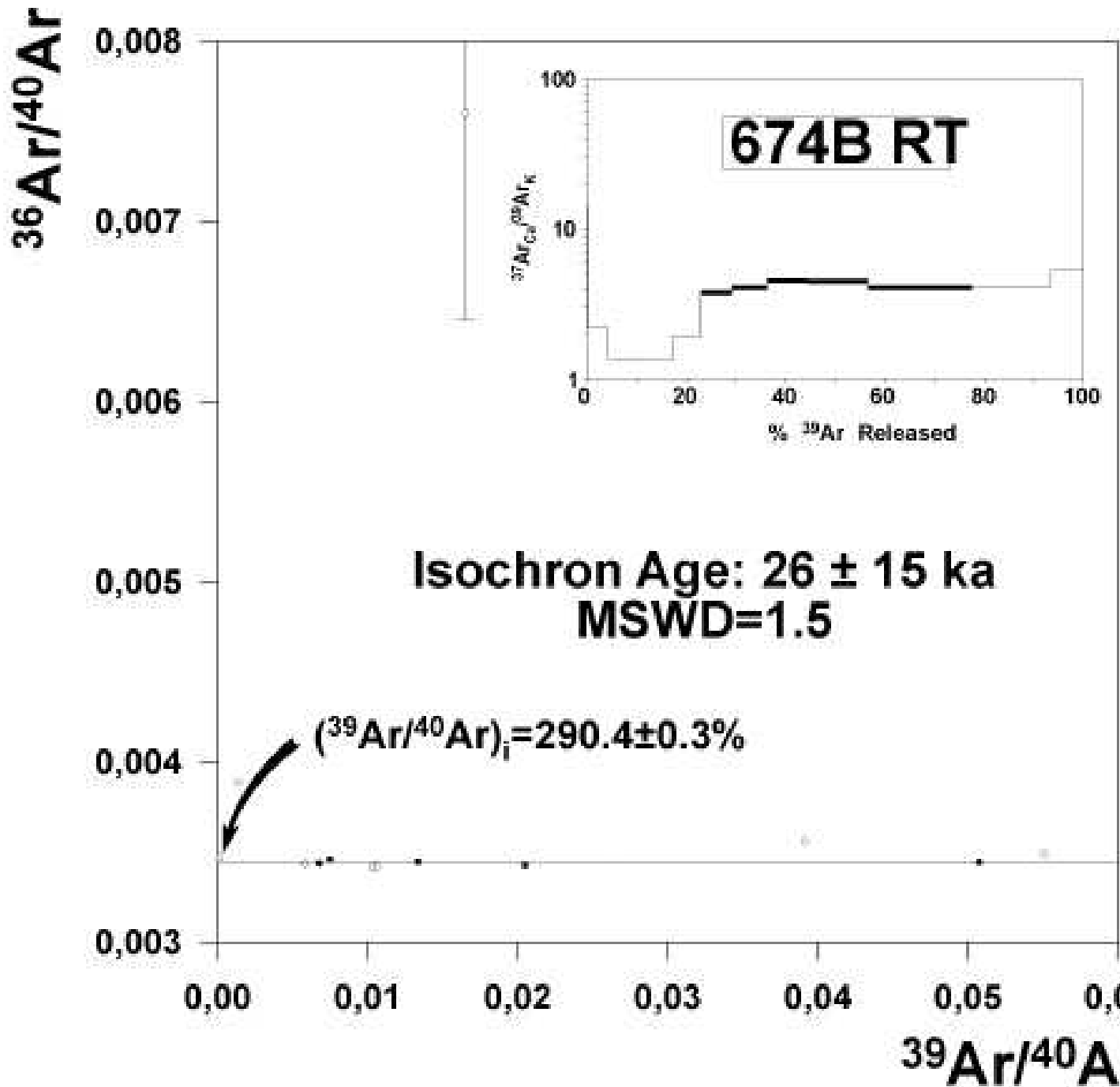


Figure 9. Isochron $^{36}\text{Ar}/^{40}\text{Ar}$ versus $^{39}\text{Ar}/^{40}\text{Ar}$ and $^{37}\text{ArCa}/^{39}\text{ArK}$ diagrams of whole rock sample 674B (Flow am1). The bold line in the Ca/K diagram defines the degassing domain used for the isochron calculation.

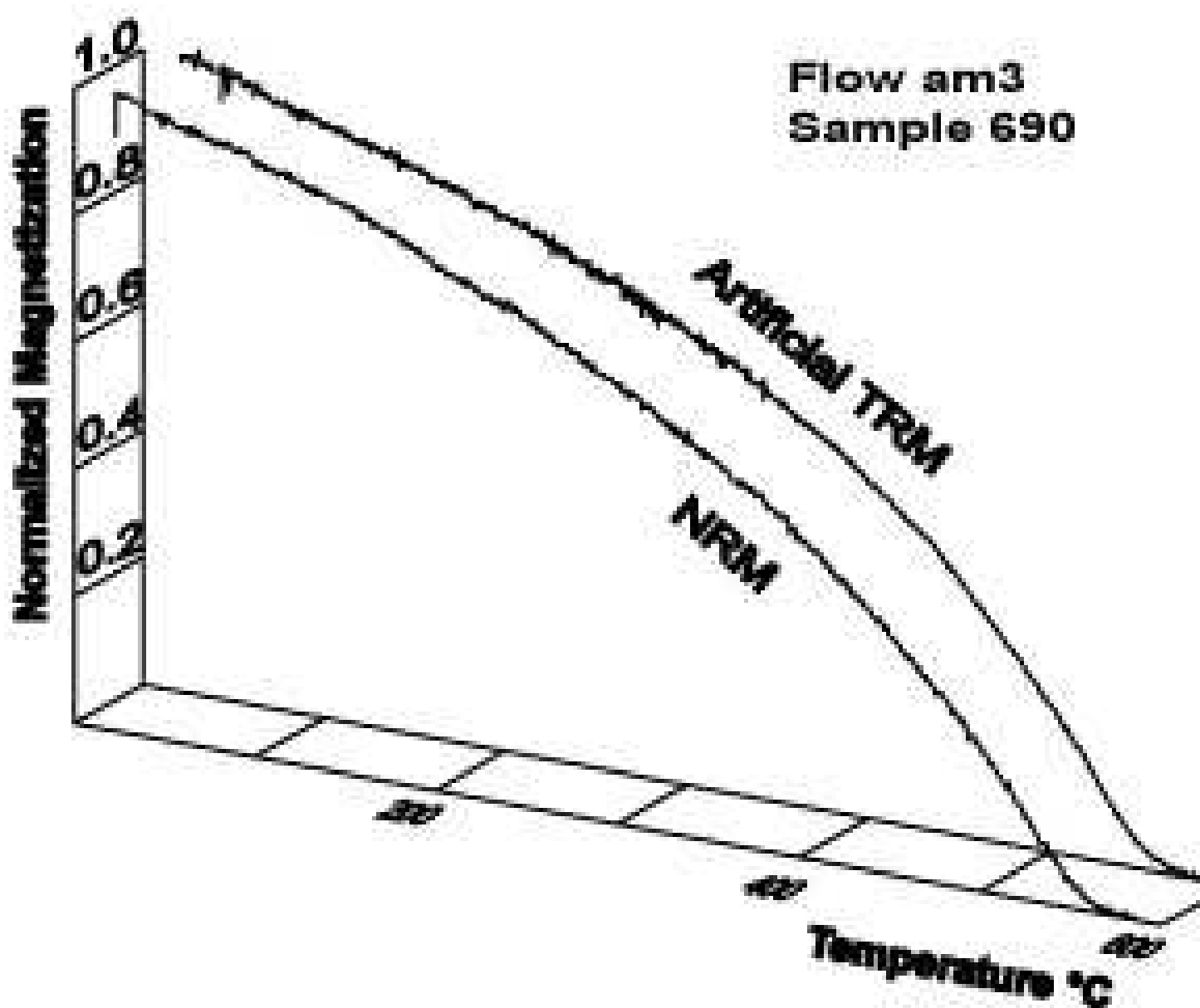


Figure 10. Comparison between thermal demagnetization of NRM and artificial total TRM.

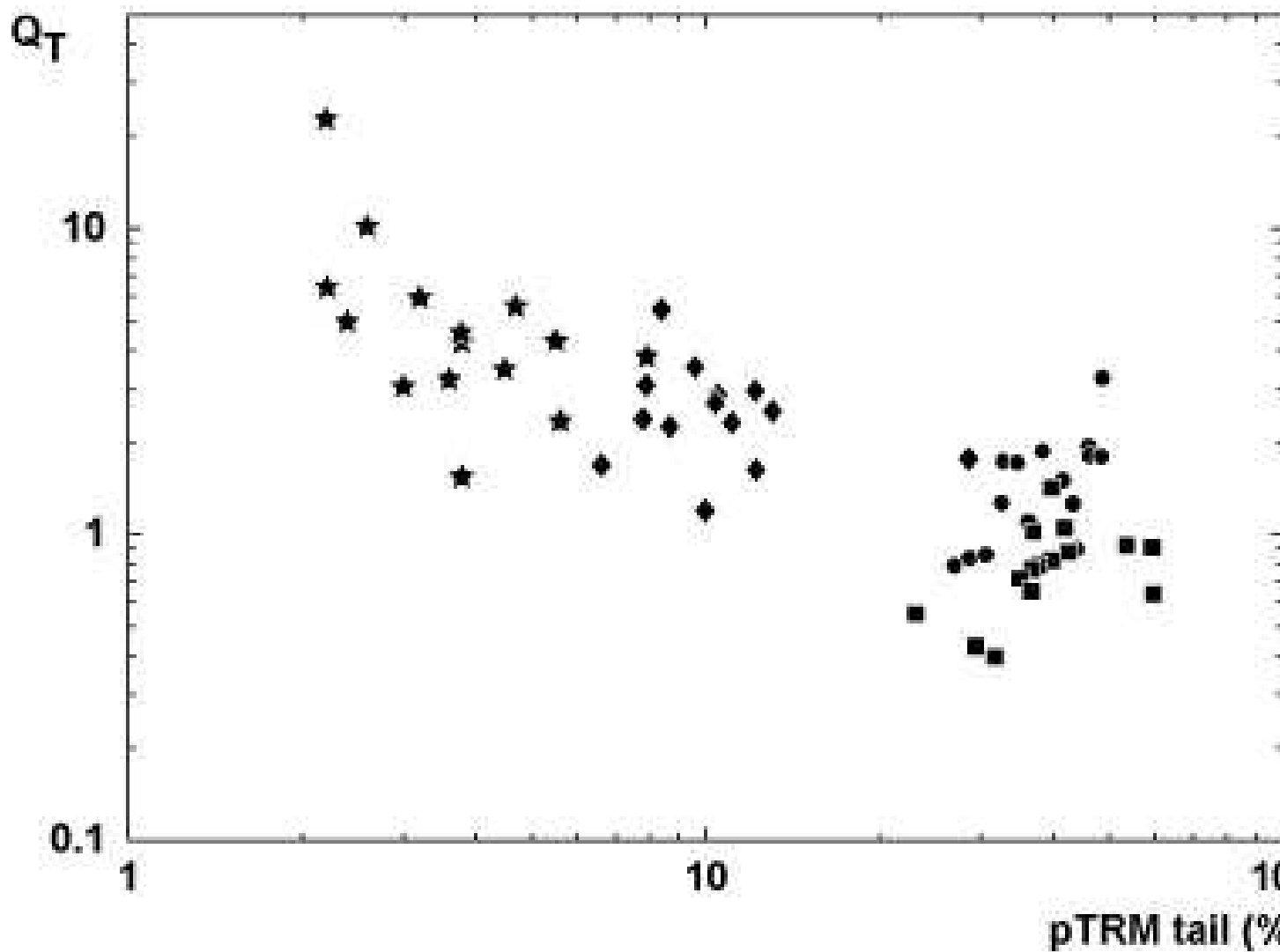
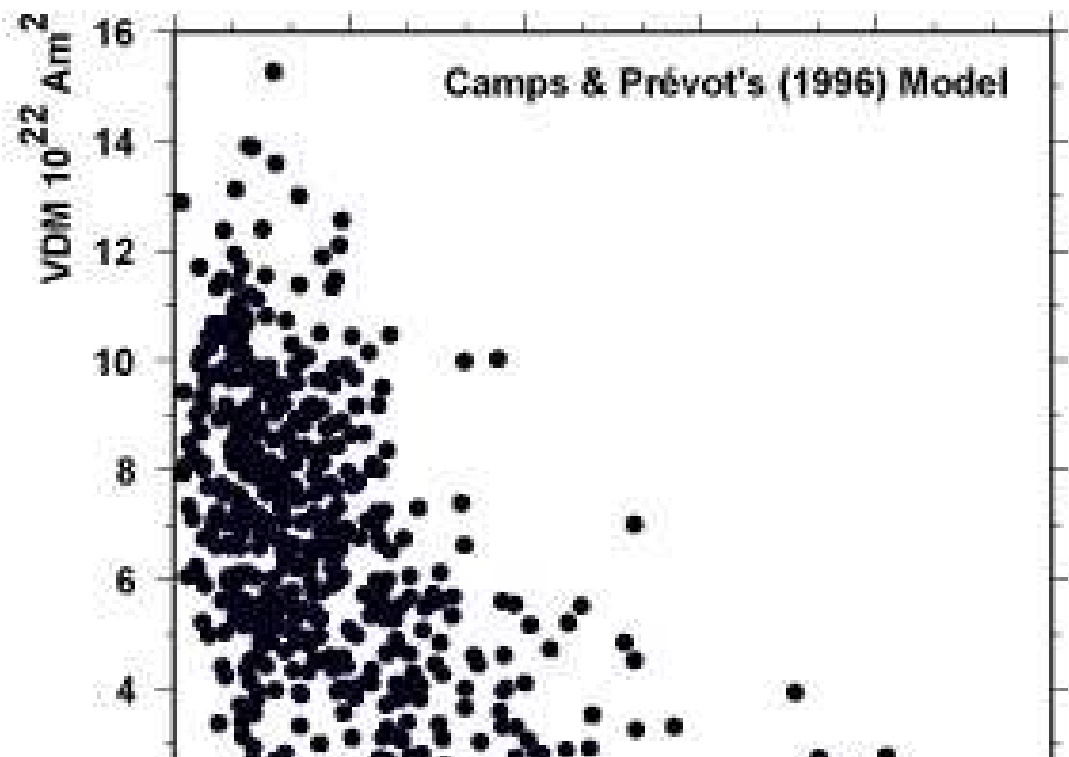
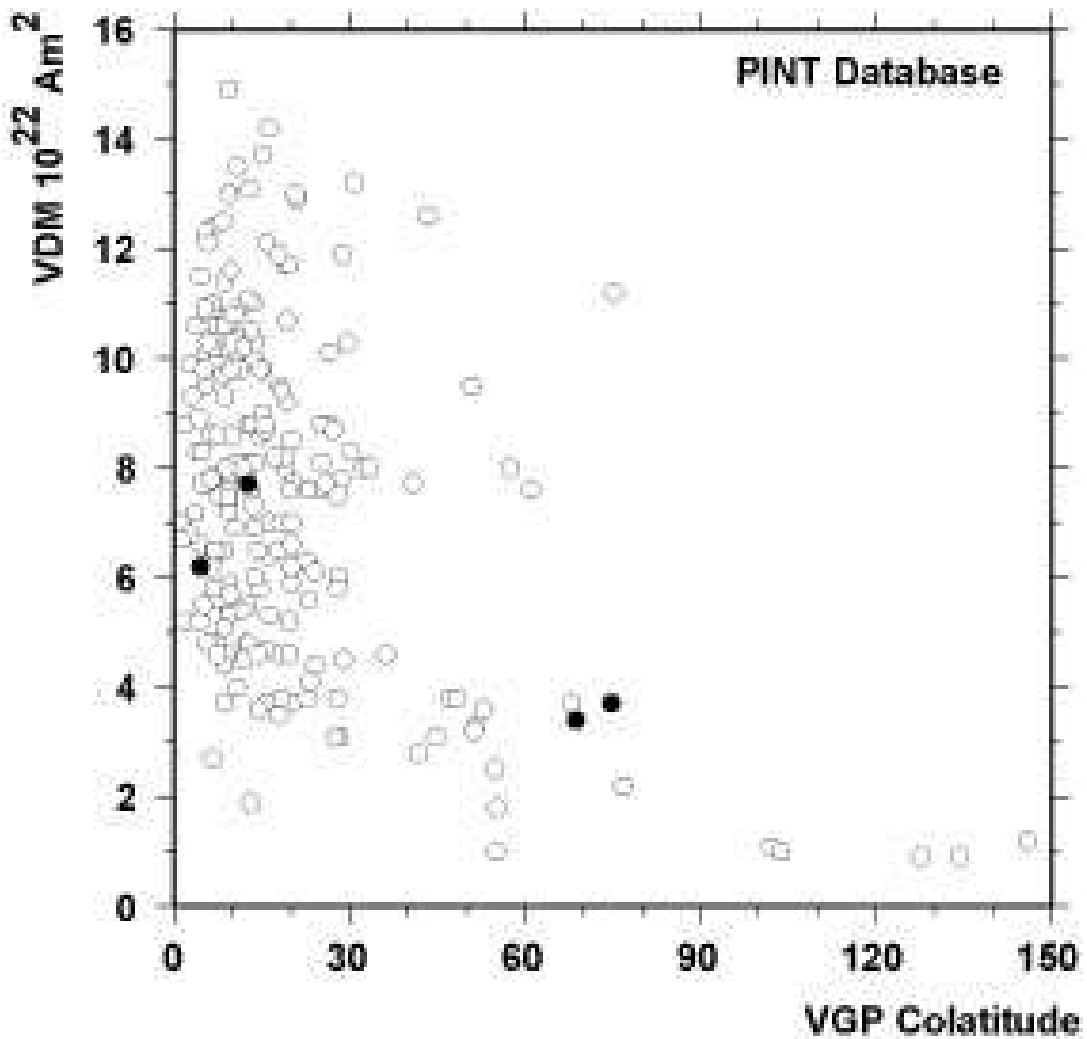


Figure 11. Log-Log plot showing the Koenigsberger ratios measured at temperature during the pTRM acquisition when the field is switched off as a function of pTRM tail [300,Troom] circles, [400,300] squares, [500,400] diamonds and [550,500] stars.



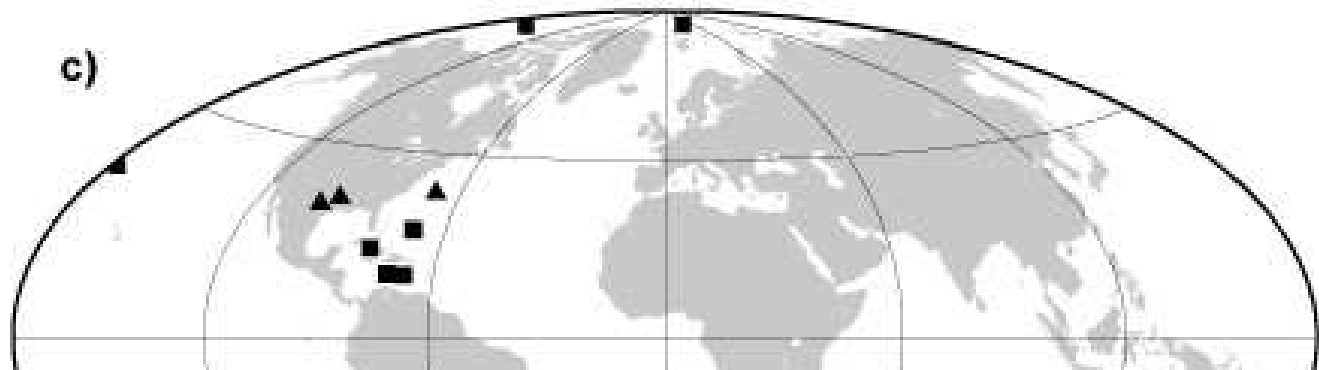
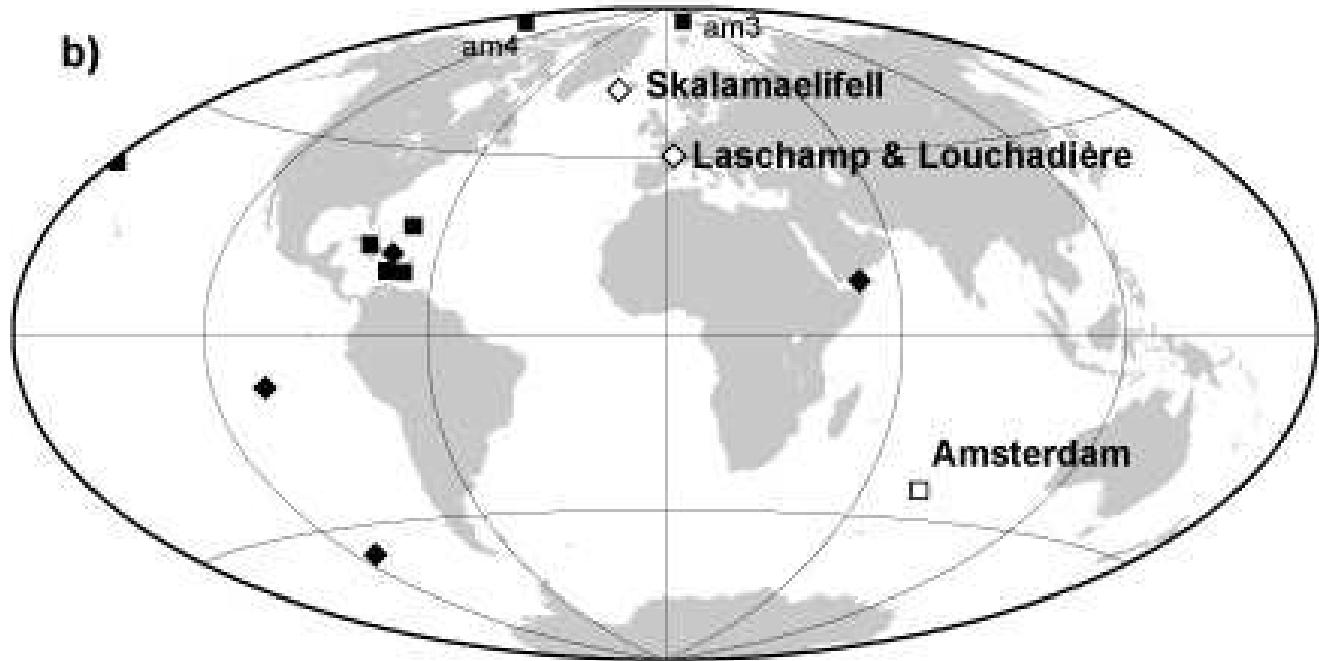
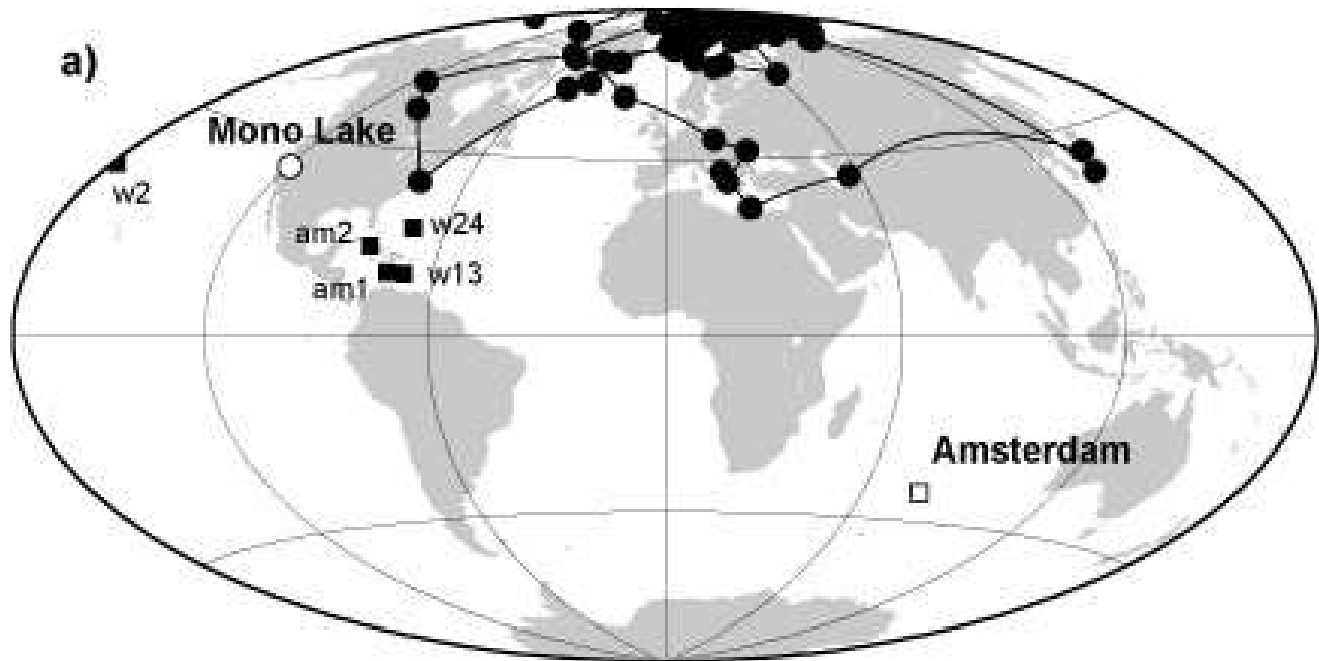


Table 1. Directional Results

Flow	n/N	Inc.	Dec.	α_{95}	κ	δ	Lat.	Long.	χ	J_{20}
am1	7/7	-70.7	238.6	5.0	144	45.6	15.2	287.8	1721.2	3.51
am2	7/7	-76.2	238.2	1.3	2287	41.6	21.2	281.1	1812.9	2.91
am3	7/8	-52.5	356.1	4.1	217	5.2	85.5	40.5	1740.4	7.95
am4	7/7	-63.1	3.9	3.8	249	9.1	77.4	205.6	661.1	6.49

n/N is the number of samples used in the analysis/total number of samples collected; Inc. and Dec. are the mean inclination positive downward and declination east of north, respectively; α_{95} and κ are the 95% confidence cone about average direction and the concentration parameter of Fisher statistics, respectively; δ is the reversal angle measured in degrees from the direction of the dipole axial field direction; Lat. and Long. are latitude and longitude of corresponding VGP position, respectively; χ is the geometric mean susceptibility ($\times 10^{-6}$ SI); J_{20} A/m is the geometric mean remanence intensity in A/m measured after a magnetic treatment of 20 mT. The flow am1 corresponds to Watkins and Nougier's (1973) flows 17 and 18 combined (see text for explanation) and am2 to their flow 19.

Table 2. Thermomagnetic and rock magnetism properties of thermally stable samples

Sample	T_C	MDF	M_{rs}/M_s	H_{cr}/H_c	300-Tr	400-300	500-400	550-500
					A (B)	A (B)	A (B)	A (B)
<i>Flow am1</i>								
668	481±21, 581±14	47	0.10	3.95	31 (13)	23 (10)	10 (33)	4 (44)
669	480±32, 540±10	30	0.06	3.72	43 (10)	60 (7)	29 (30)	8 (53)
670	394±88, 572±8	53	0.17	3.31	36 (17)	35 (14)	9 (35)	5 (34)
671	485±15, 587±20	38	0.17	8.13	29 (13)	32 (9)	12 (36)	4 (42)
673	503±38	34	n.d	n.d	27 (12)	30 (10)	7 (51)	6 (27)
674	475±11, 572±18	56	0.22	2.54	26 (nd)	26 (nd)	8 (nd)	nd (nd)
<i>Flow am2</i>								
675	473±68	27	0.25	1.76	32 (7)	37 (6)	11 (30)	2 (57)
680	516±54	23	0.19	1.83	46 (14)	60 (13)	11 (42)	3 (31)
<i>Flow am3</i>								
690	564±20	53	0.24	2.13	35 (8)	40 (7)	11 (30)	4 (55)
691	504±30, 561±17	56	0.25	1.96	38 (7)	43 (6)	12 (30)	4 (57)
692	500±9, 560±20	49	0.25	1.98	33 (7)	37 (5)	13 (27)	2 (61)
694	552±23	41	0.23	1.89	42 (5)	38 (5)	10 (24)	2 (66)
695	510±32, 561±19	48	n.d	n.d	46 (7)	53 (6)	10 (32)	3 (55)
<i>Flow am4</i>								
684	569±23	39	0.32	1.62	44 (4)	37 (5)	8 (23)	3 (68)
685	505±34, 547±7	30	n.d	n.d	49 (10)	42 (10)	8 (40)	5 (40)
686	550±10	33	n.d	n.d	48 (22)	40 (21)	8 (32)	6 (25)

T_C is the mean Curie temperature ($^{\circ}\text{C}$) calculated according to the method of Prévot et al. (1983). The confidence intervals for the Curie temperatures indicate the temperature range in which the KT curve correspond to a straight line. MDF is the Median Destructive alternating Field in mT; M_{rs}/M_s and H_{cr}/H_c are the hysteresis parameters; A values are the relative intensities measured at room temperature of the pTRM tail expressed in percent $A(T_1, T_2) = \text{tail}[\text{pTRM}(T_1, T_2)]/\text{pTRM}(T_1, T_2)$. B values shown in parentheses correspond to the percent of the total pTRM (e.g., $\sum_i \text{pTRM}_i$) each $\text{pTRM}(T_1, T_2)$ represents; intensities are measured at room temperature. nd means not determined. Note that sample 674 broke itself before the acquisition of the pTRM(550-500) was completed. Thus, we were not able to calculate B values for this sample.

Table 3. Accepted paleointensity determinations.

Flow	Sample	Fe $\pm\sigma$ Fe	T ₁ – T ₂	n	f	g	q	MAD	α	Drat	$\bar{F}_E \pm$ s.d.	VDM
am1	670D	19.5 \pm 0.6	400-570	8	0.643	0.845	16.9	6.5	2.6	5.1	24.6 \pm 3.7	3.7
	671D	27.1 \pm 0.7	400-580	9	0.688	0.867	23.1	3.8	4.7	0.9		
	673C	27.6 \pm 0.5	400-570	8	0.844	0.806	36.8	2.7	1.3	0.9		
	674C	24.3 \pm 0.6	400-570	8	0.754	0.839	27.7	3.7	1.6	0.8		
am2	675E	22.1 \pm 0.7	400-550	6	0.862	0.729	19.8	3.3	2.3	1.8	24.0 \pm 2.6	3.4
	680C	25.8 \pm 1.8	400-550	6	0.435	0.757	4.8	2.7	2.2	10.0		
am3	690B	30.3 \pm 0.6	400-580	9	0.892	0.848	35.8	3.2	1.2	2.3	32.8 \pm 2.2	6.2
	691C	34.9 \pm 0.4	400-580	8	0.925	0.755	63.2	3.4	1.3	2.3		
	692D	33.3 \pm 0.9	400-570	8	0.939	0.797	28.2	3.3	1.2	2.6		
	694D	34.9 \pm 0.8	400-570	8	0.935	0.798	34.1	4.3	1.1	2.5		
	695B	30.7 \pm 0.6	400-570	8	0.927	0.821	39.4	4.6	0.8	3.0		
am4	684E	42.3 \pm 1.4	400-550	6	0.700	0.777	16.7	3.3	2.1	2.2	46.9 \pm 4.6	7.7
	685E	47.0 \pm 0.8	400-570	7	0.758	0.742	34.4	1.7	1.5	2.6		
	686E	51.4 \pm 1.1	400-570	8	0.790	0.814	31.3	3.4	2.3	2.5		

Sample is an identifier of a sample used for the paleointensity determination; Fe is paleointensity estimate (in μT) for individual specimen, and (σ Fe) is its standard error; T₁ and T₂ are the minimum and maximum of the temperature range in $^{\circ}C$ used to determine paleointensity; n is the number of points in the T₁ – T₂ interval; f, g, and q are NRM fraction, gap factor and quality factor, respectively (Coe et al., 1978); MAD is the maximum angular deviation calculated along with the principal component for the NRM left in the T₁ – T₂ interval; α is the angle in degrees between the vector average and the principal component calculated for the NRM left in the T₁ – T₂ interval; Drat is expressed in percent and corresponds to the difference ratio between repeat pTRM steps normalized by the length of the selected NRM-pTRM segment (Selkin & Tauxe, 2000); \bar{F}_E is unweighted average paleointensity of individual lava flow and its standard deviation and VDM is the corresponding virtual dipole moment ($\times 10^{22} \text{ Am}^2$).

Table 4. Isotopic ages Results

Flow	Sample	(⁴⁰ Ar/ ³⁹ Ar) _i $\pm 2\sigma$	Isochrone age (ka \pm ka)	MSWD
am1	674B	290.4 \pm 0.8	26 \pm 15	1.5
am2	676D	288.6 \pm 1.5	18 \pm 9	0.2
am3	694F	290.2 \pm 1.2	48 \pm 22	3.2

Table 5. Laboratory Koenigsberger ratios before and after heating.

Flow	Sample	Q_L	Q'_L
am1	670D	14.4	21.7
	671D	17.9	20.4
	673C	28.0	27.8
	674C	28.6	27.9
am2	675E	39.5	34.5
	680C	8.1	8.3
am3	690B	32.2	29.3
	691C	36.1	35.4
	692D	34.8	33.7
	694D	32.2	31.7
am4	695B	30.2	29.6
	684E	42.1	41.7
	685E	37.3	29.7
	686E	33.9	27.4

Sample is the same identifier than used for the paleointensity determination; Q_L is the laboratory Koenigsberger ratio before heating; Q'_L is the Koenigsberger ratio after heating.